Improved biological performance of ketoprofen using novel modified halloysite clay nanotubes

Dounia Sid, Milad Baitiche, Lekhmici Arrar, Ferhat Djerboua, Riadh Bourzami, Pierre Alcouffe, Mokhtar Boutahala, Antonio Gil, Laurent David, Marc Le Borgne

Improved biological performance of ketoprofen using novel modified halloysite clay nanotubes

Dounia Sid[a,b], Milad Baitiche[a,*], Lekhmici Arrar[c], Ferhat Djerboua[a], Riadh Bourzami[d], Pierre Alcouffe[e], Mokhtar Boutahala[f], Antonio Gil[g], David Laurent[e], Marc Le Borgne[b,h,*]

[a] *Laboratoire de Préparation, Modification et Applications des Matériaux Polymériques Multiphasiques, Département de Génie des Procédés, Faculté de Technologie, Université Ferhat Abbas Sétif 1, Sétif 19000, Algérie*

[b] *EA 4446 Bioactive Molecules and Medicinal Chemistry, SFR Santé Lyon-Est CNRS UMS3453 - INSERM US7, Université Claude Bernard Lyon 1, Univ Lyon, Lyon, 69373, France*

[c] *Laboratory of Applied Biochemistry, Faculty of Nature and Life Sciences, University Ferhat Abbas Setif 1, Setif, 19000, Algeria*

[d] *Research unit of emergent materials, Université Ferhat Abbas Sétif 1, Sétif, 19000, Algérie*

[e] *Ingénierie des Matériaux Polymères (IMP), CNRS, UMR 5223, 15 Boulevard Latarjet, Université Claude Bernard Lyon 1, Univ Lyon, F-69622, Villeurbanne, France*

[f] *Laboratoire de Génie des Procédés Chimiques (LGPC), Département de Génie des Procédés, Faculté de Technologie, Université Ferhat Abbas Sétif 1, Sétif 19000, Algérie*

[g] *INAMAT[2], Science Department, Los Acebos Building, Public University of Navarra, Campus of Arrosadía, 31006, Pamplona, Spain*

[h] *Small Molecules for Biological Targets Team, Centre de recherche en cancérologie de Lyon, Centre Léon Bérard, CNRS 5286, INSERM 1052, Université Claude Bernard Lyon 1, Univ Lyon, Lyon, 69373, France*

*Corresponding authors.

Email addresses: baitiche_milad@yahoo.fr (Milad Baitiche), marc.le-borgne@univ-lyon1.fr (Marc Le Borgne).

Highlights

- Halloysite was modified by citric acid to obtain new clay nanotubes.
- Clay nanotubes were loaded with ketoprofen.
- Halloysite, modified halloysite and their corresponding formulations were fully characterized.
- New formulations exhibited promising anti-inflammatory and analgesic activities.
- Total protective effect against gastric damage was observed with ketoprofen-loaded modified halloysite clay nanotubes.

Abstract:

In the present work, elegant modification of halloysite (Hal) by citric acid (CA) was realized. The corresponding novel bio-composite (Hal-CA) was then used as drug carrier. To validate this concept, ketoprofen (KET), a known non-steroidal anti-inflammatory agent, was chosen as drug model. KET has low solubility and a short biological half-life, which can cause some limitations in its therapeutic use. In addition, its use is limited due to gastrointestinal side effects. All Hal, Hal-CA, Hal-KET and Hal-CA-KET samples were characterized using several techniques such as X-ray diffraction (XRD), Fourier transform infrared (FTIR) spectroscopy, transmission electron microscopy (TEM), N2 adsorption-desorption, thermogravimetric analysis (TGA) and differential scanning calorimetry (DSC). The release of KET from the prepared formulations was investigated at pH 1 and 6.8 by means of UV-Visible spectroscopy. In addition, kinetics of the release of KET from inclusion complexes were determined by fitting the release profiles to the first order, Korsmeyer–Peppas and Higuchi models. In order to assess these novel bio-composites, anti-inflammatory and anti-nociceptive activities were also evaluated *in vivo*. Finally, the ulcerogenic activity and the histopathological effects of all formulations were compared to that of pure KET. This work showed the increase of the anti-inflammatory and antinociceptive potentials of KET loaded in Hal-CA, as well as a maximum protection against ulcers. This suggests that Hal-CA can be considered as a new carrier for pharmaceutical formulations.

Keywords: Halloysite; Ketoprofen; Citric acid; Bio-composites; Release; *In vivo* performance

1. Introduction

Ketoprofen (KET) is a non-steroidal anti-inflammatory drug (NSAID) belonging to the class of 2-arylpropionic acids, well known for its analgesic, anti-inflammatory and antipyretic properties (Kantor, 1986). It is indicated mainly for the symptomatic treatment of pain and inflammation of osteoarthritis and rheumatoid arthritis (Freitas et al., 2018). In recent years, possible new therapeutic benefits of KET are gaining interest. The drug has proven its effectiveness in the prevention of the development of various cancers including colorectal and lung cancers as well as in the treatment of neurodegenerative disorders among which Alzheimer and Parkinson's diseases (Rençber et al., 2009). However, the use of KET is limited due to a

large number of side effects; especially those related to gastrointestinal (GI) complications, abdominal pain, constipation and flatulence observed in more than 3% of patients (Kantor, 1986). In addition, its low solubility (0.05 mg·mL^{-1} at 25 °C in water), its short biological half-life ($t_{1/2}$= 2-4 h) lead to a low bioavailability of this active pharmaceutical ingredient (API). However, in order to overcome this drawback, high doses are recommended (maximum dose 300 mg per day) with a variable frequency of administration (2 to 4 times per day). High doses naturally increase the risk of developing side effects, limiting long-term use (Cerciello et al., 2015). For all these reasons, KET is a potential candidate for new development of controlled release formulations, capable of providing drug release systems with a predetermined rate and time (Joussein et al., 2005), having an improved solubility, and eventually reducing its well-known harmful effects. So far, many host materials were studied with KET such as synthetic polymers (Mangindaan et al., 2012), layered double hydroxides (San Román et al., 2012), biopolymers (Maestrelli et al., 2015; Matos Fonseca et al., 2019), cyclodextrins (Zhao et al., 2019), UiO-66 metal-organic frame (Li et al., 2019).These systems have been prepared by different methods, including intercalation, inclusion, mixing and kneading, and were then tested for their release properties of the guest ingredient.

Clay minerals have been used for different biomedical purposes since many years and new studies were recently published (Charaabi et al. 2019; Charaabi et al., 2021). Additionally, a particular attention is also given to halloysite (Hal) (Joussein et al., 2005). Hal is extracted from natural deposits with a natural aluminosilicate composition having a hollow nanotubular structure and formed by rolled kaolin sheets. The external diameter of the Hal tubes ranges typically from 50 to 200 nm with an internal diameter of 5 to 30 nm and a length of 0.5 to 25 µm. Hal nanotubes contain up to 10 to 15 rolled aluminosilicate layers with a repeat distance of 0.72 nm between layers (Yendluri et al., 2017a). The crystalline and chemical composition of Hal are similar to those of kaolinite but Hal can be intercalated by a monolayer of water molecules increasing the basal spacing. Thus, Hal mainly occurs in two different polymorphs, the hydrated form (basal distance around 1.0 nm) with the formula $Al_2Si_2O_5(OH)_4.2H_2O$ and the dehydrated form (basal distance about 0.7 nm) with the formula $Al_2Si_2O_5(OH)_4$, identical to kaolinite. The outer surface of Hal nanotubes is composed mainly of negatively charged SiO_2 moieties and an inner surface composed of positively charged Al_2O_3 groups. In addition, Hal nanotubes have a high specific surface area and a good thermal stability. They are inert and chemically stable in a wide range of pH (3-10), non-toxic, biocompatible, abundant and low cost (Liu et al., 2014; Alipoormazandarani et al., 2015; Tharmavaram et al., 2018; Oliyaei et al., 2019). An important advantage of Hal clays, as compared with platy clays such as

montmorillonite, kaolin and laponite, is that Hal do not need exfoliation and can be easily dispersed in water. For this, Hal nanotubes have been widely considered as supports for the encapsulation and release studies of medicines, inorganic salts, APIs, antiseptics, corrosion inhibitors, antibacterials, cosmetic additives, enzymes and proteins (Abdullayev and Lvov, 2016). On top of these applications, Hal was employed in numerous fields as a catalyst support (Massaro et al., 2017; Huang et al., 2021), as a filler for hydrogels and polymers (Bertolino et al., 2018), as composite bioplastics (Lisuzzo et al., 2020), as an adsorbent of pollutants (Xia et al., 2021). In addition, Hal nanotubes coated with octadecyltrimethoxysilane were investigated, their cellular uptake was confirmed and no apoptosis-inducing effect was observed on cells (Rozhina et al., 2020). It is now well established that Hal can fix active molecules through three different ways: (i) adsorption onto the external and internal walls of nanotubes, (ii) encapsulation in the internal space (lumen of the nanotubes) and (iii) intercalation between the layers (Abdullayev and Lvov, 2013). It has also been shown that the encapsulation in the internal space is the main mode for water-soluble active principles and this already allows a high capacity and a controlled release (Abdullayev and Lvov, 2013). A number of APIs has been encapsulated in Hal nanotubes, including 5-aminosalicylic acid (Aguzzi et al., 2013), ibuprofen (Tan et al., 2013), diclofenac (Lisuzzo et al., 2019), dexamethasone (Veerabadran et al., 2007), oflaxacin (Aguzzi et al., 2013), nifedipine (Yendluri et al., 2017b), furosemide (Hanif et al., 2016), diphenhydramine (Hemmatpour et al., 2015), 5-fluorouracil (Harikrishnan et al., 2020), resveratrol (Vergaro et al., 2012) and paclitaxel (Yendluri et al., 2017a). All of these drugs are sparingly soluble in water; therefore, intercalation in Hal nanotubes plays a major role in sustained release, but also ensures an effective dispersion in aqueous media. However, the practical applications of Hal are restricted by its rather low exchange capacity, due to the low degree of isomorphic substitution of silicium (Si) by aluminum (Al) in the tetrahedral layer, which leads to a low content and rapid release of molecules intercalated in Hal (Yang et al., 2016). For example, when Hal is used as an unmodified support, only a weak affinity may be observed between Hal and APIs. In order to improve the performance of Hal, the properties of internal and/or external surfaces of this later should be adapted. In general, the modification of the surface relates to the introduction of functional groups on the surface of the Hal (e.g. surfactants, silanes, octadecyl phosphonic acid, polyethyleneimine) (Massaro et al., 2018). However, the toxicity and the cost of these modifying products limit their application in the modification of Hal. Therefore, it is essential to find a gentle, environmentally-friendly modifier to functionalize the Hal without compromising the drug's intercalation effectiveness.

Citric Acid (CA) is a natural organic acid commonly used as cross-linking agent. CA has three acid dissociation constants, namely pKa1 = 3.13 (H_2Cit^{1-}), pKa2 = 4.76 ($HCit^{2-}$) and pKa3 = 6.40 (Cit^{3-}). In a neutral aqueous solution, CA is completely ionized in its citrate form (Cit^{3-}) (Apelblat and Barthel, 1991). As a tricarboxylic acid, CA cross-linked materials have effective functional groups (-OH and -COOH). In recent years, certain biomaterials (e.g. bentonite) modified by CA have been proposed in the literature (Schilling et al., 2008; Ghorpade et al., 2016, 2017, 2018; Zhang et al., 2019).

In the present work, we consider the active role of Hal and Hal treated with CA (Hal-CA) as friendly drug carriers for KET. Such drug delivery systems (DDS) can assist in overcoming the side effects associated with KET by designing new oral DDS that can limit drug release in the stomach and enhance the release in the intestine. This may improve the drug efficiency together with the patient compliance. Further we detail the multi-step procedure used for the purification of the natural crude Hal. At this stage, it is possible to prepare organic/inorganic material (Hal-CA) using an esterification reaction between surface OH groups of Hal and COOH groups of CA (Sajab et al., 2011; Tcheumi et al., 2019; Zhang et al., 2019). Two formulations (Hal-KET and Hal-CA-KET) were produced and compared. KET loading and release kinetics were also investigated. All biomaterials and formulations were characterized by different techniques such as X-ray diffraction (XRD), Fourier transform infrared (FTIR) spectroscopy, transmission electron microscopy (TEM), N2 adsorption-desorption, thermogravimetric analysis (TGA) and differential scanning calorimetry (DSC). Release studies of formulations and their kinetics were also investigated. Finally, all formulations were evaluated for their pharmacological effects. *In vivo* studies on the anti-inflammatory and analgesic activities, after oral administration of Hal-KET and Hal-CA-KET, have been carried out on rodents. The ulcerogenic activity and histopathological effects of the formulations were also compared to that of pure KET.

2. Materials and methods

2.1. Materials

The raw halloysite material was obtained from the mine of Djebbel Debbagh (Guelma, Algeria). The mineral was first milled in a mortar, sieved at 45 µm and dried at 100 °C for 24 h. The drug ketoprofen (abbreviated as KET) (molecular formula: $C_{16}H_{14}O_3$, CAS number 22071-45-4, MW: 254.3 g·mol^{-1}, pKa= 4.4, log K_{OW}= 3.00, water solubility at 25 °C =21 mg·L^{-1}), was supplied by SALEM pharmaceutical Laboratories, El- Eulma, Algeria. Citric acid (CA) (2-hydroxypropane-1,2,3-tricarboxylic acid, CAS number 77-92-9, solubility in water 59.2%

w/w at 20 °C) was purchased from Sigma Aldrich, USA. Lambda carrageenan was purchased from Sigma Aldrich. All other used chemicals are of analytical grades. All reagents are used as received.

2.2. Halloysite purification

The first step in the purification of the raw halloysite material consists in the removal of the water-soluble matter. To this end, 20 g of the material are dispersed in 1 L of distilled water and stirred for 24 h at room temperature. Then the suspension is centrifuged at 5000 rpm for 5 min. In order to remove the carbonates, the resulting powder was further suspended treated under vigorous stirring with 2 L 0.1 M HCl at room temperature for 4 h (Bergaya and Lagaly, 2013). After a second centrifugation the obtained precipitate was repeatedly washed with distilled water and centrifuged successively for five times to eliminate chloride ions (tested by $AgNO_3$ solution). Further purification consists in the elimination of the soil organic matter and this was achieved through a further treatment when submitting the solid residue to the action of an aqueous solution of (10% v/v) hydrogen peroxide (1 L) and stirred overnight at room temperature. Then, the residual hydrogen peroxide was degraded by heating the suspension at 70 °C for 30 min. The precipitate was washed with hot water (100 °C, 1 L) and dried for 24 h at 50 °C. The material was milled in a mortar, sieved at 45 µm, kept in a bottle and stored away from moisture. The resultant sample was denoted as Hal.

2.3. Preparation of halloysite modified by citric acid

A mixture of the Hal (1 g), CA (3 g, used as surface functionalization agent) and sodium dihydrogen phosphate (2 g, used as catalytic agent) was added to 25 mL of distilled water in a round bottom flask. Then, the suspension was heated at 100 °C under magnetic stirring for 1 h. The mixture was then cooled down to room temperature and sequentially washed three times with (150 mL) portions of distilled water. The obtained residue was collected by centrifugation, dried at 50 °C for 24 h; the Hal-CA sample was obtained as a white solid, milled in a mortar, sieved at 45 µm and stored at 4 °C in an airtight container.

2.4. KET loading

In order to obtain a saturated solution, a total of 1 g of KET was added in 250 mL of water. Then, 1 g of either Hal or Hal-CA was added to the solution and mixed to obtain a homogeneous suspension. This later was placed in vacuum (600 mbar) for 4 cycles and for 30 min each. According to the most recent studies, the vacuum steps induced an optimization of

the loading efficiency due to water removal from the inner cavity of Hal (Lisuzzo et al., 2021 and 2019). Then the solution entered the lumen to ensure maximum loading. The solid samples were recovered by centrifugation and washed three times with 200 mL portions of water to remove excess of non-retained drug. The samples were dried overnight, milled in a mortar, sieved at 45 µm and stored at 4 °C in an air-tight container. The samples were denoted Hal-KET and Hal-CA-KET.

2.5. Characterization techniques

X-ray diffraction (XRD) analysis for the Hal, Hal-CA, Hal-KET and Hal-CA-KET samples was performed using a Bruker D8 advance diffractometer operating at 40 kV and 30 mA with Cu Kα1 radiation (λ = 0.15418 nm). Radial scans were recorded in the reflection scanning mode from 2θ = 5 to 80° with a scanning rate of 10°/min. Bragg's law, defined as $n\lambda = 2\,d\sin\theta$, was used to compute the inter-reticular distance (d) for the examined clay samples. The mean diameter of crystallite found in Hal material is evaluated by Scherrer equation ($D = k\lambda/\beta\cos\theta$), where k is the shape factor close to 0.9, β is the width at half height of the reflection peaks, λ is the incident wavelength and 2θ is the Bragg angle.

FTIR study was carried out using Shimadzu Ftir-8400 spectrophotometer having a standard mid-IR DTGS detector. FTIR spectra were recorded in the range of 400–4000 cm^{-1} using the KBr pellets technique.

TEM investigations were performed with a JEOL JEM-1400 Flash electron microscope at "Centre Technologique des Microstructures de l'Université de Lyon 1", operating with an accelerating voltage of 120 kV. A droplet of 5 µL of Hal nanoparticles dispersed in distilled water was deposited onto a carbon coated copper grid (CF200-CU UL EMS). Excess solution was carefully blotted off using filter paper. The sample was air-dried at room temperature during one night before imaging.

Nitrogen gas adsorption–desorption isotherms were measured using a Micromeritics ASAP 2020 Plus Version 1.03 at 77 K. The measurements were taken after degassing the samples under vacuum at 120 °C for 3 h. The specific surface areas (S_{BET}) are determined according to the BET method at the relative pressure in the range of 0.05–0.35. The total pore volume (Vp) was directly determined from the nitrogen adsorption at $P/P_o = 0.99$. The pore diameter (Dp) was obtained by the formula: $Dp = 4Vp/S_{BET}$ (Brunauer et al., 1938; Sahnoun et al., 2016).

Finally, thermogravimetric analysis/differential scanning calorimetry (TGA/DSC) were conducted on an EXTAR 6000 thermal analyzer (Seiko, Mahwa, NJ, USA) under the nitrogen

flow of 15 $cm^3 \cdot min^{-1}$ for the sample and 10 $cm^3 \cdot min^{-1}$ for the balance. The samples were heated from 30 to 900 °C, with a rate of 10 $°C \cdot min^{-1}$.

2.6. In vitro drug release studies

In vitro release experiments of the KET from Hal, Hal-CA and pure KET were performed using the United States Pharmacopeia Paddle Method (Apparatus II) on Heidolph RZR 2041. The samples loaded with 50 mg of KET (i.e. 249.6 mg of Hal-KET and 193.8 mg of Hal-CA-KET) were placed into a hard gelatin capsules (size 00), and then soaked into 900 mL of simulated gastric medium (0.1 M HCl, i.e. pH 1) for 2 h. Then the acid medium was drained and replaced by 900 mL 0.01 M KH_2PO_4 buffer solution adjusted to pH 6.8 with 0.1 M NaOH, as simulated intestinal fluid. Temperature was maintained at 37 ± 0.5 °C during the entire release process and the release medium was stirred at 100 rpm. At suitable time intervals, 1 mL of the suspension medium was aliquoted, using a syringe, and filtered through 0.22 μm nylon disc filters. Then, an equivalent volume of fresh medium was added in order to maintain sinking conditions. The KET concentration was determined from the peak at 256 nm using an UV-Vis spectrophotometer (SHIMADZU UV-1800). Each drug release test was carried out in duplicate.

In addition, kinetics of the release of KET from inclusion complexes were determined by fitting the release profiles to the first order (equation 1) (Wagner, 1969), Korsmeyer–Peppas (equation 2) (Kim and Fassihi, 1997) and Higuchi (equation 3) (Higuchi et al., 1963) theoretical models, as follows:

$$F_t = 1\text{-}\exp(-K_1.t), \quad (1)$$

Where F_t is the fraction of drug released at time t in the medium and K_1 is the first order release constant.

$$F_t = K_{KP} t^n, \quad (2)$$

Where K_{KP} is the Korsmeyer–Peppas constant, and n is the release exponent indicative of the drug release mechanism.

$$F_t = K_H t^{0.5} + a, \quad (3)$$

Where K_H is the Higuchi release constant and “a” is a constant characterizing the initial drug fraction.

Then, the selection of the best fit model is based on the regression coefficient value R^2.

2.7. Animals preparation

In this part of the study, male Swiss albino mice of 20-30 g weight and male Wistar rats of 150-200 g were used. These animals are brought from 'Institut Pasteur' of Algeria. Before the beginning of the experimentation, the animals were kept in polycarbonate cages for 7 days under ordinary laboratory conditions (12/12 h light/dark cycle, at 23 ± 2 °C with free food and water access).

2.8. Carrageenan-induced rat paw edema

To assess the *in vivo* anti-inflammatory effectiveness of the formulations (Hal-KET and Hal-CA-KET) in comparison with the pure drug, 24 male Wistar rats were distributed into four groups with six rats each. Therefore, the rats were kept under fasting overnight prior for conducting the experiments except water was fed, 2 mL solution of saline (0.9%, w/v) was administered orally to group I (control group), KET equivalent to body weight of 5 $mg \cdot kg^{-1}$ and dissolved in 2 mL solution of saline was introduced by gavage to group II (standard group), Hal-KET and Hal-CA-KET formulations equivalent to drug 5 $mg \cdot kg^{-1}$ body weight were administered orally to the groups III and VI (test groups), respectively, using 2 mL of NaCl (0.9%) solution.

An acute inflammation (edema) was instigated one hour after the administration of the pure drug and formulations. For this, we injected 0.1 mL of 1% (w/v) lambda carrageenan in saline into the sub-plantar zone of each Wistar rat's right-hand paw (Boppana et al., 2016). After the phlogistic agent has been injected, the volume of the paw was measured by a digital caliper at 0 h, every h for 6 h and finally at 24 h. The average increase in paw volume relatively to control animals can estimate edema. Therefore, the anti-inflammatory activity was determined by the percentage of edema reduction in treated rats in relation to controls as shown in the following equation:

$$\text{Inhibition } \% = \frac{(Vc\text{-}Vt)}{Vc} * 100, \qquad (4)$$

Where Vc is changed in paw size of control and Vt is changed in treated paw size.

2.9. Acetic acid-induced writhings

Male Swiss mice (25-30 g, n = 6/group) were orally treated with NaCl 0.9% solution (control), KET, Hal-KET and Hal-CA-KET (5 $mg \cdot kg^{-1}$ of drug) before the intraperitoneal injection of 0.6% of acetic acid (100 µL/10 g). The analgesic activity was determined by the number of abdominal constrictions counted for 30 min (Cunha et al., 2016) and the % writhing inhibition was calculated using the following formula:

$$\%MPE = \frac{(\text{Mean no. of constrictions (control) - Mean no. of constriction (test)})}{\text{Mean number of constrictions (control)}} * 100, \quad (5)$$

Where MPE is the percentage of maximum possible effect.

2.10. Ulcerogenicity study

For this part, the rats were under fasting and separately kept in wire mesh cages to avoid coprophagy except water was fed during 24 h prior to the start of experiments. Table 1 summarized the experimental design and animal groups. On the morning of the tests, magnetic agitation was used to achieve a well-dispersed suspension of pure drug and samples. Then 2 mL of gavage solutions equivalent to 500 mg per kg (body weight) of KET was then given orally for each fasted rat (Laudanno et al., 2000). After 6 h, each rat was sacrificed. The stomach was then removed and opened up along the greater curvature, gently washed by dipping in the saline solution.

Then total area of the lesions and total area of the stomach were measured using AUTOCAD-2018 software. The percentage of ulceration is calculated according to the following formula:

$$\%\ \text{ulceration} = \frac{\text{total lesion area}}{\text{total stomach area}} * 100, \quad (6)$$

2.11. Histopathological examinations and assessments

Stomach sections were fixed in 10% formalin, then stomach tissues were processed by dehydration using xylene and ethanol then they were embedded in paraffin and then serially-sectioned (3-µm thick) using a Leica RM2135 microtome (Leica, Berlin, Germany), installed on glass slides and colored with hematoxylin and eosin (H&E) solution. The photographs were taken using binocular light microscope (CXRIII, Labomed, Mumbai, India).

2.12. Statistical analysis

Graph Pad Prism (version 8.3.0 for Windows) was used to carry out statistical test analysis. All *in vivo* results were indicated as mean ± standard error of mean (SEM). A one-way variance analysis (ANOVA) followed by Dunnet's test was used to analyze each assay. The *p*-values less than 0.05 were considered statistically significant.

3. Results and discussion

3.1. Characterization of the purified Hal

3.1.1. Powder x-ray diffraction

The XRD diagram of Hal is shown in Fig. 1(a). The results confirmed that Hal was not pure and traces of other minerals (e.g. alunite, quartz) coexisted with. The pattern showed the characteristic diffraction peaks at the angular positions 2θ = 12.3, 20.2, 25.0, 30.0, 35.3, 36.2, 55.3 and 62.6°. According to the powder diffraction file (JCPDS 29-1487) of 7 Å-Hal, these eight angular positions are related to the Miller indices of the reticular plane families (001), (020), (002), (113), (003), (200), (211) and (-3-31), respectively. In addition, the inter-reticular distances [d(001) =7.33 Å and d(020) = 4.41 Å] are characteristic of the dehydrated phase of 7 Å-Hal with the chemical formula $Al_2Si_2O_5$ having a tubular morphology (Yuan et al., 2012). The XRD pattern also illustrates the existence of trace of quartz, formed by the dissociative SiO_2 that segregated from the 7 Å-Hal. Its weak peaks are indexed by letter Q and are located at the six angular positions 10.2, 26.6, 39.2, 40.5, 45.5 and 47.8°. According to the diffraction file (JCPDS 78-2315), these peaks are related to the hexagonal phase planes of SiO_2(100), (1-1-1), (1-1-2), (2-20), (02-1) and (2-12), respectively (Segovia-Sandoval et al., 2018). Another phase is also observed which corresponds to alunite and indexed by letter A. Its four characteristic peaks are observed at the angular positions of 15.6, 18.0, 50.9 and 52.4°. These peaks are attributed to the (003), (100), (033) and (200) reflexions, respectively, according to JCPDS 73-1652. Moreover, the crystallite seizes of Hal, quartz and alunite, are estimated using Scherrer method (Tan et al., 2013). Their values are close to 15.2, 13.1 and 11.7 nm, respectively, and when comparing the intensities, the main crystalline phase is that of the Hal.

3.1.2. FTIR spectroscopy

In the FTIR spectrum of Hal (Fig. 1(b)), two bands centered at 3692 and 3626 cm^{-1}, were attributed to the O-H stretching of the inner surface and the inner layers, respectively. In addition, the wide bands centered at 3464 cm^{-1} and the weak one at 1639 cm^{-1} were attributed to the O-H stretching and O-H deformation vibrations of the physically adsorbed water, respectively (Sabahi et al., 2018). The groups at 1090 cm^{-1} and 1029 cm^{-1} corresponded to the stretching vibrations of Si-O and Si-O-Si, respectively. The band at 916 cm^{-1} was attributed to the O-H deformation of the internal O-H groups, and the one at 793 cm^{-1} was caused by a symmetrical stretching vibration of Si-O. The bands at 752 and 687 cm^{-1} were attributed to the perpendicular Si-O stretching vibrations. The three remaining bands at 540, 470, and 437 cm^{-1} were attributed to the deformation vibrations of the groups Al-O-Si, Si-O-Si, and Si-O,

respectively (Yuan et al., 2012). As a result, both X-ray diffraction and FTIR analyses confirmed the expected structure of Hal.

3.1.3. TEM analysis

The TEM image of Hal clearly showed that HAL particles have a typical cylindrical shape with a transparent central cylindrical area parallel to the tube axis (Fig. 1(c)), indicating that the particles are hollow and open-ended. Various sizes of the nanotubules were present in the sample, their lengths ranged from 40 to 1300 nm, and their widths from 25 to 85 nm. The size distribution of Hal reported in this study may be specific to the mine of Djebbel Debbagh (Guelma, Algeria) but it stays in the same order of magnitude than the other Hal obtained from other sources (Joussein et al., 2005b).

3.1.4. N2 adsorption-desorption analysis

The N2 adsorption-desorption isotherm of the Hal was presented in Fig. 1(d). The isotherm of this sample is classified as type II with H3 hysteresis loops, on the basis of IUPAC recommendations. The H3 hysteresis loop observed in this case where the adsorbent forms aggregates can be attributed to capillary condensation taking place in a non-rigid texture and is not characteristic of a defined mesoporosity (Greg et al., 1962; Torres et al., 1999). The S_{BET}, V_{pore} and Dp values of Hal are 18.93 $m^2 \cdot g^{-1}$, 0.0576 $cm^3 \cdot g^{-1}$ and 11.8 nm, respectively.

3.1.5. Thermogravimetric analysis

The TGA analysis for Hal showed two significant mass losses clearly observed (Fig. 1(e)). The first mass loss takes place from 50 to 200 °C, and is attributed to the dehydration of physically adsorbed water and interlamellar residual water (8% water content). The second loss of mass between 300 and 600 °C corresponds to a derivative thermogravimetry (DTG) peak centered at 480 °C. It can be attributed to the structural dehydration of the aluminol groups (Al-OH). This result is similar to that observed in the literature concerning the dehydroxylation of Hal between 400 and 600 °C (Yuan et al., 2012).

3.2. Characterization of the CA–modified and KET-loaded halloysite samples

3.2.1. Powder x-ray diffraction

The XRD diagrams of the Hal-CA, KET and composites (Hal-KET and Hal-CA-KET) are displayed in Fig. 2. The 2θ-positions of the XRD reflection peaks of Hal-CA are almost

unchanged compared to those of Hal. Nevertheless, the treatment with CA impacts the crystallinity of Hal, this result can be observed directly on the pattern by a marked decrease of the relative peak intensities. Moreover, the CA addition decreased the crystallite size of the Hal from 15.20 to 8.56 nm. In addition, the pattern of KET powder showed a crystalline structure. The most significant diffraction peaks are observed at angular positions of 2θ = 13.4, 14.8, 18.8, 23.3, 28.2 and 29.9°. These values are in fair agreement with previous results (Cervini-Silva et al., 2013). Otherwise, the Hal-CA-KET pattern illustrates the appearance of KET diffraction peaks at the angular positions of 2θ = 13.4, 14.8, 18.8 and 23.3°. This confirms that the crystalline form of the molecular KET is not affected, while this crystalline structure is lost when KET is directly deposited on the unmodified Hal. This phenomenon probably shows that CA promotes the incorporation/adsorption of KET on Hal and further heterogeneous nucleation of KET crystals happens. In addition, the crystalline structure of Hal was poorly affected. This may be explained by the fact that KET is not interspersed in the interlamellar spacing, but rather deposited on the internal and external surfaces of Hal (Carretero and Pozo, 2010). Previously, the intercalation of organic molecules in Hal has been shown to depend on several factors, namely (i) the charge, the size of the organic molecule and the number of functional groups and (ii) the state of hydration of Hal (inter-lamellar water promoting further intercalation of organic molecules) (Tan et al., 2013). In our case, Hal is dehydrated and KET only exhibits one COOH group per molecule. These two characteristics do not favor the intercalation of KET in Hal. Comparable result was obtained concerning the intercalation of ibuprofen in Hal nanotubes (Tan et al., 2013).

3.2.2. FTIR spectroscopy

The interaction between KET and Hal or Hal-CA was further evaluated by FTIR spectroscopy (Fig. 3). The previously published spectrum of CA alone showed a broad band centered at 3291 cm^{-1} due to the stretching vibrations of the valence of OH (Segovia-Sandoval et al., 2018). Moreover, the peaks at 1725 cm^{-1}, 1400 cm^{-1} and 1222 cm^{-1} are due to the stretching vibrations of the carbonyl groups of CA. For the Hal-CA sample, in addition to the specific bands of Hal, the spectrum showed new bands characteristic of CA at 1765, 1735 and 1384 cm^{-1}. The peak at 1725 cm^{-1} (CA) moved to 1765 cm^{-1} (Hal-CA), thus demonstrating the functionalization of Hal through ester-type bonds (Sajab et al., 2011; Zhang et al., 2019). The spectrum of KET FTIR displayed characteristic adsorption peaks at 1698 cm^{-1} (C=C stretching of carboxylic acid), 1654 cm^{-1} (stretching of ketone group attached to two aromatic rings), 1598 cm^{-1} and 1440 cm^{-1} (C=C stretching from the aromatic ring), 1321 cm^{-1} (CH deformation of

CH_3 symmetrical) and 1281 cm^{-1} (C=C deformation of aromatic rings). Concerning the Hal-KET and Hal-CA-KET samples, new peaks at 1691 cm^{-1}, 1660 cm^{-1}, 1450 cm^{-1} and 1290 cm^{-1}, belonging to KET, were observed. These shifted bands confirm that the KET molecules have been adsorbed from the surfaces of Hal and Hal-CA. The interaction mechanisms between key groups of KET and Hal / Hal-CA (COOH, OH, Si-OH, Al-OH) should involve hydrogen bonds and/or Van der Waals interactions. These results are similar to that of 5-aminosalicylic acid and ibuprofen adsorbed on the external and internal surfaces of Hal (Aguzzi et al., 2013; Tan et al., 2013).

3.2.3. TEM analysis

Fig. 4 shows the TEM images of Hal-KET, Hal-CA and Hal-CA-KET. Comparatively to the image of the Hal (Fig. 1(c)), the external diameter of Hal-KET and Hal-CA-KET was not significantly affected by the deposit of KET (Fig. S1). This result can conclude that the KET molecules were not inserted in the interlamellar spacing (Tan et al., 2013) although a change of the contrast in the lumen parts was observed on the TEM images of Hal-KET (Fig. 4(a)). Comparatively to Hal, this variation of the contrast confirms the presence of different electronic densities and may be related to the existence of KET molecules in the lumen.

Furthermore, the TEM images of Hal-CA and Hal-CA-KET present black spots (Fig. 4 (b) and (c)), illustrating that the surface of Hal was modified by CA-addition without a loss of the tubular morphology, and also, a slight degradation of the Hal was observed after the deposit treatment of CA and KET, these results are in good agreement with the XRD data.

3.2.4. N2 adsorption-desorption analysis

Fig. 5 shows the adsorption–desorption isotherms of N2, at 77 K, for the Hal-KET and Hal-CA-KET samples. The two isotherms are similar and belong to type II isotherms. This is characteristic of mesoporous/macroporous solids according to IUPAC classification, with H3 hysteresis loops. This indicates the presence of tubular pores (open at both ends) or of capillaries with an ink-well shape (San Roman et al., 2016). After activation of Hal with CA, the Hal surface area significantly decreases from 18.93 to 0.635 $m^2 \cdot g^{-1}$ (Figure not shown). This shows an interaction between CA and Hal indicating that the CA was inserted inside the pores interacting with the hydroxyl groups. After addition of KET, the S_{BET} and Vp values of the Hal-KET and Hal-CA-KET samples were increased. The corresponding values of S_{BET} and V_P are 40.7 $m^2 \cdot g^{-1}$ and 0.193 $cm^3 \cdot g^{-1}$ for Hal-KET and then 64.6 $m^2 \cdot g^{-1}$ and 0.296 $cm^3 \cdot g^{-1}$ for Hal-CA-KET. Furthermore, the pore diameter (Dp) increased from 11.8 nm (Hal) to 18.6 for Hal-KET

and 18.0 nm for Hal-CA-KET. This change may have been due to the formation of micropores during surface breakage, resulting from structural rearrangement or transformation (Yuan et al., 2012). Moreover, the values of 18.6 and 18.0 nm are of the same order of the internal diameter of the Hal (Tan et al., 2013).

3.2.5. Thermogravimetric analysis

The thermogravimetry analysis (TGA) of Hal-CA, Hal-KET and Hal-CA-KET samples is shown in Fig. 6. The thermograms of CA and KET show thermal decompositions between 122-286 °C and 217-394 °C, respectively (Fig. S2). Under N_2 flow, they are fully decomposed into CO_2 and H_2O. These TGA profiles indicate that CA and KET should be considered as thermally stable up to 131 and 167 °C, respectively. The mass losses of Hal-KET and Hal-CA-KET show different profiles in comparison with pure Hal: the degradation profiles of KET, CA and Hal are largely impacted by the presence of the other constituents and resulting interactions. In particular, the degradation temperatures of KET in the two composites Hal-KET and Hal-CA-KET are shifted to higher temperatures in comparison with that of pure KET (Fig. 6). This strongly suggest that KET has been adsorbed in Hal and is more stable (Sabahi et al., 2018). KET degradation occurs above 500 °C, whereas the degradation peak is close to 480 °C for the pristine Hal. It is also observed that the remaining water content (determined from the mass loss between 20 and 200 °C) for the materials Hal-CA, Hal-KET and Hal-CA-KET are 5.80, 3.82 and 6.80%, respectively. These values are lower compared to pure Hal (10.71%). This evidences the replacement of free and bound water from Hal by CA in Hal-CA and KET in Hal-KET and Hal-CA-KET. The total mass losses at 800 °C are 20.3, 20.2, 40.3 and 46% for the samples Hal, Hal-CA, Hal-KET and Hal-CA-KET, respectively. The increase in mass losses from pure Hal and Hal-CA to about 40-46% for Hal-KET and Hal-CA-KET is clearly due to the thermal degradation of KET retained by the aluminosilicate structure of the Hal. The intercalated quantities of KET in the Hal-KET and Hal-CA-KET samples are approximately 20 and 26%, respectively. These values were calculated using the following equations:

KET from HAL-KET % = (mass loss in HAL-KET) - (mass loss in HAL), (7)

And

KET from HAL-CA-KET % = (mass loss in HAL-CA-KETO) - (mass loss in HAL-CA), (8)

These amounts adsorbed in Hal and Hal-CA are close to the amounts of other APIs adsorbed in Hal mentioned in the literature (Aguzzi et al., 2013; Abdullayev and Lvov, 2016). It is noted that the loading efficiency of active agents in clays can vary from 20 to 30%.

3.3. In vitro drug release studies from unmodified and modified Hal

KET was successively released at pH 1 and then at pH 6.8 as displayed in Fig. 7. In fact, loading of KET in Hal and Hal-CA delayed the drug-release compared to the drug alone. Indeed, the cumulative release of KET from natural Hal was about 83% after 90 min. After treated with CA, an evident delay in the cumulative release to 34% after 90 min was clearly observed.

At pH 1, the release of KET from the two formulations showed two stages, including a fast-bust release followed by a subsequent prolonged release. The fast release can be ascribed to the externally adsorbed KET, because the surface-loaded KET was weakly bonded through hydrogen bonding. The prolonged release of KET in Hal-KET can be ascribed to the release of the lumen-loaded KET, of which the diffusion was substantially delayed by the pseudo one-dimensional nanotube structure of Hal (Tan et al., 2013).

For the release of KET from CA-modified Hal, it is clearly observed that the burst release of KET was attenuated, and the prolongated release rate of KET was slower. The reason is the stronger interactions (hydrogen bonds) between KET and CA-modified Hal which delayed the dissolution and diffusion of KET from CA-modified Hal (Tan et al., 2013). Interestingly, pH impacted the release of KET with a faster release when the pH value of the medium reached 6.8. For Hal-KET and Hal-CA-KET, KET-release kinetics from Fig. 7 were fitted using three mathematical models as described in the literature (Costa and Sousa Lobo, 2001; Costa et al., 2003; Dash et al., 2010). The best results were obtained with the Korsmeyer–Peppas model and are given in Table 2. Then KET demonstrates a quasi-Fickian release behavior ($n<0.5$) which indicates minimal interaction between KET and Hal-KET or Hal-CA-KET (Dantas de Freitas et al., 2018).

3.4. Carrageenan-induced rat paw edema

The carrageenan-induced paw edema is a popular test used in the screening of potential drugs and their corresponding formulations for anti-inflammatory activity. Results from the study indicate that pure KET caused 44% and 16% of paw edema inhibition at 3 h and 24 h, respectively (Fig. 8, Table S1).

KET-loaded Hal had greater anti-inflammatory effects than pure KET (Fig. 8, Table S1). Indeed, Hal-KET caused 63% and 39% of paw edema inhibition at 3 h and 24 h. This can be explained by a slower release of KET from Hal. With Hal-KET, the maximum inhibitory effect is obtained between 3 and 5 h, with a median value around 63%. This inhibitory effect is even more spectacular with the use of the Hal-CA-KET formulation, with inhibition values between

68% (3 h) and 70% (24 h) (Fig. 8, Table S1). The overall improvement of the anti-inflammatory effect is due to an initial fast release of KET from Hal-CA during the first h (inhibition effect at 70%) and a subsequent slower release able to provide an effective concentration of KET for 24 h (with a maximum 85% at 5 h) (Table S1). Another issue is that simple Hal and Hal-CA formulations apparently also have their own anti-inflammatory effect (Cornejo-Garrido et al., 2012; Cervini-Silva et al., 2013). Between 2 and 24 h, the effect of Hal and Hal-CA is similar, around 20% inhibition (Fig. S3, Table S1). These observations strongly indicate that the Hal-CA-KET system is highly efficient for reducing inflammation, with a maximum inhibition of 83% between 4 and 5 h. This effect is maintained until 24 h, with 70% inhibition (only 16% for KET alone).

3.5. Acetic acid-induced writhings

The treatment with Hal and Hal-CA clay nanotubes by oral administration removed writhings and enhancing the anti-nociceptive effect, with values between 41% and 30% for Hal and Hal-CA, respectively (Fig. S4). KET alone reduced writhings by 83%, on the other hand, a maximum effect of 100% both with Hal-KET and Hal-CA-KET (Fig. 9).

3.6. Ulcerogenicity study

A systematic macroscopic examination of all rat stomach (n = 24) was performed. For each group, a typical representative image of the stomach (fundus-corpus) is shown (Fig. 10). Negative control group displayed a healthy corpus (Fig. 10(a)), whereas the KET administration generated well-defined hemorrhagic streak ulcers (Fig. 10(b)) with a maximum percentage of ulceration area close to 11% (Fig. 11).

Hal-KET demonstrated a significant protective effect of stomach (Fig. 10(c)) in comparison with KET-treated rats, with also only 0.3% of ulceration (Fig. 11). Nevertheless, Hal-CA-KET provided the total mucosa protection (Fig. 10(d)). In addition, it is important to note that Hal and Hal-CA may adhere to the GI mucous membrane and then protect the stomach wall (e.g. by increasing the viscosity and stability of the gastric mucus) (Carretero and Pozo, 2010; Awad et al., 2017).

3.7. Histopathological studies

Histopathological studies were conducted in rats. It was observed no gastric damage in the negative control group (saline) as shown in Fig. 12($a_{1,2}$). In the positive control group (KET), necrotic gastric mucosa was found with external hemorrhages and deeply penetrated

injuries into the gastric epithelium (Fig. 12($b_{1,2}$)). Severe congestion, dilated blood vessels (Fig. 12(b_3)) and infiltration of neutrophil inflammatory cells (Fig. 12(b_4)) were also present. On the other hand, KET-loaded Hal decreased the pathological structure of the gastric mucosa when compared with those of the KET group (Fig. 12($c_{1,2}$)). Nevertheless, histopathological examination revealed that stomach tissue showed sub-mucosal congestion and mild inflammation (Fig. 12($c_{1,2}$)). In the case of KET-loaded Hal-CA, histopathological examination revealed that stomach tissue showed normal gastric mucosa (Fig. 12($d_{1,2}$)). The results of macroscopic and microscopic observations were then strongly correlated.

4. Conclusions

The present study successfully endorsed the development and evaluation of a novel formulation which ensures both the increase in the therapeutic effectiveness of KET and a decrease in the gastric damage related to its main side effects. Hal and Hal-CA were found to be a convenient and reliable nanoscale carrier platform for loading of KET. In addition, results of the physicochemical characterization confirmed the interaction between HAL-CA and KET, both in the luminal space and external surfaces. *In vitro* release kinetics of the Hal-CA clay nanotubes revealed an effective release for 24 h. *In vivo* studies indicated clearly that the treatment of animals with formulations reduced carrageenan-induced paw edema and the number of writhings induced by acetic acid. Moreover, Hal-CA-KET provides a total gastric mucosa protection. Hal-CA can be considered as a promising and credible tool for future pharmaceutical formulations.

Declaration of competing interest

The authors report no conflicts of interest.

Ethics statement

The animal studies were carried out after getting the clearance of the Ethics Committee of the Université Ferhat Abbas Sétif 1 (ref. CED/01/03-2019), and the experiments were conducted in strict compliance following the ethical principles provided by the Committee for the Purpose of Control and Supervision of Experiments on Animal (CPCSEA).

Acknowledgements

The authors are very grateful to “Ministère de l’Enseignement Supérieur et de la Recherche Scientifique de l’Algérie”, PROFAS B+ doctoral scholarship, University of Ferhat

Abbas Sétif 1 as well as University Claude Bernard Lyon 1 for the funding and the support of the project. Our thanks go to SALEM Pharmaceutical Laboratories headed by Dr. A. Maiza for the supply of the different chemicals used in this study. Pr. M. Boutahala is gratefully acknowledged for the provision of the equipment used in the analyses as well as the laboratory facilities. Dr. A. Gil also thanks Santander Bank (Navarra, Spain) for funding via the Research Intensification Program. The authors wish to acknowledge the helpful suggestions made by Mrs. Christine Janssen.

References

Abdullayev, E., Lvov, Y., 2016. Chapter 22 - Halloysite for Controllable Loading and Release, in: Yuan, P., Thill, A., Bergaya, F. (Eds.), Developments in Clay Science, Nanosized Tubular Clay Minerals. Elsevier, pp. 554–605. https://doi.org/10.1016/B978-0-08-100293-3.00022-4.

Abdullayev, E., Lvov, Y., 2013. Halloysite clay nanotubes as a ceramic "skeleton" for functional biopolymer composites with sustained drug release. J. Mater. Chem. B 1, 2894–2903. https://doi.org/10.1039/C3TB20059K.

Aguzzi, C., Viseras, C., Cerezo, P., Salcedo, I., Sánchez-Espejo, R., Valenzuela, C., 2013. Release kinetics of 5-aminosalicylic acid from halloysite. Colloids Surf. B Biointerfaces 105, 75–80. https://doi.org/10.1016/j.colsurfb.2012.12.041.

Alipoormazandarani, N., Ghazihoseini, S., Mohammadi Nafchi, A., 2015. Preparation and characterization of novel bionanocomposite based on soluble soybean polysaccharide and halloysite nanoclay. Carbohydr. Polym. 134, 745–751. https://doi.org/10.1016/j.carbpol.2015.08.059.

Apelblat, A., Barthel, J., 1991. Conductance studies on aqueous citric acid. Z. Naturforsch. A 46, 131–140. https://doi.org/10.1515/zna-1991-1-222.

Awad, M.E., López-Galindo, A., Setti, M., El-Rahmany, M.M., Iborra, C.V., 2017. Kaolinite in pharmaceutics and biomedicine. Int. J. Pharm. 533, 34–48. https://doi.org/10.1016/j.ijpharm.2017.09.056.

Bergaya, F., Lagaly, G., 2013. Chapter 7.1 - Purification of Natural Clays, in: Bergaya, Faïza, Lagaly, Gerhard (Eds.), Developments in Clay Science, Handbook of Clay Science. Elsevier, pp. 213–221. https://doi.org/10.1016/B978-0-08-098258-8.00008-0.

Bertolino, V., Cavallaro, G., Lazzara, G., Milioto, S., Parisi, F., 2018. Halloysite nanotubes sandwiched between chitosan layers: a novel bionanocomposite with multilayer structure. New J. Chem. 42, 8384–8390. https://doi.org/10.1039/C8NJ01161C.

Boppana, R., Kulkarni, R.V., Mohan, G.K., Mutalik, S., Aminabhavi, T.M., 2016. In vitro and in vivo assessment of novel pH-sensitive interpenetrating polymer networks of a graft copolymer for gastro-protective delivery of ketoprofen. RSC Adv. 6, 64344–64356. https://doi.org/10.1039/C6RA04218J.

Brunauer, S., Emmett, P. H, Teller, E., 1938. Adsorption of gases in multimolecular layers. J. Am. Chem. Soc. 60, 309–319. https://doi.org/10.1021/ja01269a023.

Carretero, M.I., Pozo, M., 2010. Clay and non-clay minerals in the pharmaceutical and cosmetic industries Part II. Active ingredients. Appl. Clay Sci. 47, 171–181. https://doi.org/10.1016/j.clay.2009.10.016.

Cerciello, A., Auriemma, G., Morello, S., Pinto, A., Del Gaudio, P., Russo, P., Aquino, R.P., 2015. Design and in vivo anti-inflammatory effect of ketoprofen delayed delivery systems. J. Pharm. Sci. 104, 3451–3458. https://doi.org/10.1002/jps.24554.

Cervini-Silva, J., Nieto-Camacho, A., Palacios, E., Montoya, J.A., Gómez-Vidales, V., Ramírez-Apán, M.T., 2013. Anti-inflammatory and anti-bacterial activity and cytotoxicity of halloysite surfaces. Colloids Surf. B Biointerfaces 111, 651–655. https://doi.org/10.1016/j.colsurfb.2013.06.056.

Charaabi, S., Tchara, L., Marminon, C., Bouaziz, Z., Holtzinger, G., Pensé-Lhéritier, A., Le Borgne, M., Issa, S., 2019.A comparative adsorption study of benzophenone-3 onto synthesized lipophilic organosilicate, Laponite and montmorillonite. Appl. Clay Sci. 170, 114–124. https://doi.org/10.1016/j.clay.2019.01.005.

Charaabi, S., Absi, R., Pensé-Lhéritier, A., Le Borgne, M., Issa, S., 2021. Adsorption studies of benzophenone-3 onto clay minerals and organosilicates: Kinetics and modelling. Appl. Clay Sci. 202, 105937. https://doi.org/10.1016/j.clay.2020.105937.

Cornejo-Garrido, H., Nieto-Camacho, A., Gómez-Vidales, V., Ramírez-Apan, M.T., del Angel, P., Montoya, J.A., Domínguez-López, M., Kibanova, D., Cervini-Silva, J., 2012. The anti-inflammatory properties of halloysite. Appl. Clay Sci. 57, 10–16. https://doi.org/10.1016/j.clay.2011.12.001.

Costa, F.O., Sousa, J.J.S., Pais, A.A.C.C., Formosinho, S.J., 2003. Comparison of dissolution profiles of ibuprofen pellets. J. Control. Release, 89, 199–212. https://doi.org/10.1016/S0168-3659(03)00033-6.

Costa, P., Sousa Lobo, J.M., 2001. Modeling and comparaison dissolution profiles of ibuprofen pellets. Eur. J. Pharm. Sci., 13, 123–133. https://doi.org/10.1016/s0928-0987(01)00095-1.

Cunha, V.R.R., Guilherme, V.A., de Paula, E., de Araujo, D.R., Silva, R.O., Medeiros, J.V.R., Leite, J.R.S.A., Petersen, P.A.D., Foldvari, M., Petrilli, H.M., Constantino, V.R.L., 2016. Delivery system for mefenamic acid based on the nanocarrier layered double hydroxide: Physicochemical characterization and evaluation of anti-inflammatory and antinociceptive potential. Mater. Sci. Eng. C 58, 629–638. https://doi.org/10.1016/j.msec.2015.08.037.

Dantas de Freitas, E., Pires Rosa, P.R., Carlos da Silva, M.G., Adeodato Vieira, M.G., 2018. Development of sericin/alginate beads of ketoprofen using experimental design: Formulation and *in vitro* dissolution evaluation. Powder Technol. 335, 315–326. https://doi.org/10.1016/j.powtec.2018.05.016.

Dash, S., Murphy, P.N., Nath, I., Chowdhury, P., 2010. Kinetic modeling on drug release from controlled drug delivery systems. Acta Pol. Pharm., 67, 217–223.

Freitas, E.D. de, Rosa, P.C.P., Silva, M.G.C. da, Vieira, M.G.A., 2018. Development of sericin/alginate beads of ketoprofen using experimental design: Formulation and in vitro dissolution evaluation. Powder Technol. 335, 315–326. https://doi.org/10.1016/j.powtec.2018.05.016.

Ghorpade, V.S., Yadav, A.V., Dias, R.J., 2017. Citric acid crosslinked β-cyclodextrin/carboxymethylcellulose hydrogel films for controlled delivery of poorly soluble drugs. Carbohydr. Polym. 164, 339–348. https://doi.org/10.1016/j.carbpol.2017.02.005.

Ghorpade, V.S., Yadav, A.V., Dias, R.J., 2016. Citric acid crosslinked cyclodextrin/hydroxypropylmethylcellulose hydrogel films for hydrophobic drug

delivery. Int. J. Biol. Macromol. 93, 75–86. https://doi.org/10.1016/j.ijbiomac.2016.08.072.
Ghorpade, V.S., Yadav, A.V., Dias, R.J., Mali, K.K., Pargaonkar, S.S., Shinde, P.V., Dhane, N.S., 2018. Citric acid crosslinked carboxymethylcellulose-poly(ethylene glycol) hydrogel films for delivery of poorly soluble drugs. Int. J. Biol. Macromol. 118, 783–791. https://doi.org/10.1016/j.ijbiomac.2018.06.142.
Gregg, S.J., Sing, K.S.W., 1982. Adsorption, surface area and porosity. 2nd ed. Academic Press, London. https://doi.org/10.1002/bbpc.19820861019.
Hanif, M., Jabbar, F., Sharif, S., Abbas, G., Farooq, A., Aziz, M., 2016. Halloysite nanotubes as a new drug-delivery system: a review. Clay Miner. 51, 469–477. https://doi.org/10.1180/claymin.2016.051.3.03.
Harikrishnan, S., Sedev, R., Beh, C.C., Priest, C., Foster, N.R., 2020. Loading of 5-fluorouracil onto Halloysite nanotubes for targeted drug delivery using a subcritical gas antisolvent process (GAS). J. Supercrit. Fluids 159, 104756. https://doi.org/10.1016/j.supflu.2020.104756.
Hemmatpour, H., Haddadi-Asl, V., Roghani-Mamaqani, H., 2015. Synthesis of pH-sensitive poly (N,N-dimethylaminoethyl methacrylate)-grafted halloysite nanotubes for adsorption and controlled release of DPH and DS drugs. Polymer 65, 143–153. https://doi.org/10.1016/j.polymer.2015.03.067.
Huang, J., Zhang, Y., Zhang, Y., 2021. Preparation and characterization of manganese oxides supported on functionalized halloysite nanotubes with enhanced catalytic oxidation for toluene. Appl. Clay Sci. 209, 106147. https://doi.org/10.1016/j.clay.2021.106147.
Joussein, E., Petit, S., Churchman, J., Theng, B., Righi, D., Delvaux, B., 2005. Halloysite clay minerals - a review. Clay Miner. 40, 383–426. https://doi.org/10.1180/0009855054040180.
Kantor, T.G., 1986. Ketoprofen: A review of itspharmacologic and clinicalproperties. Pharmacotherapy 6, 93–102. https://doi.org/10.1002/j.1875-9114.1986.tb03459.x.
Kim, H., Fassihi, R., 1997. Application of binary polymer system in drug release rate modulation. 2. Influence of formulation variables and hydrodynamic conditions on release kinetics. J. Pharm. Sci. 86, 323–328. https://doi.org/10.1021/js960307p.
Laudanno, O.M., Cesolari, J.A., Esnarriaga, J., San Miguel, P., Bedini, O.A., 2000. In vivo selectivity of nonsteroidalantiinflammatorydrugs and gastrointestinal ulcers in rats. Dig. Dis. Sci. 45, 1359–1365. https://doi.org/10.1023/A:1005508120776.
Li, Z., Zhao, S., Wang, H., Peng, Y., Tan, Z., Tang, B., 2019. Functional groups influence and mechanism research of UiO-66-type metal-organic frameworks for ketoprofen delivery. Colloids Surf. B Biointerfaces 178, 1–7. https://doi.org/10.1016/j.colsurfb.2019.02.027.
Lisuzzo, L., Cavallaro, G., Milioto, S., Lazzara, G., 2019. Layered composite based on halloysite and natural polymers: a carrier for the pH controlled release of drugs. New J. Chem. 43, 10887–10893. https://doi.org/10.1039/C9NJ02565K.
Lisuzzo, L., Cavallaro, G., Milioto. S., Lazzara, G., 2020. Effects of halloysite content on the thermo-mechanical performances of composite bioplastics, Appl. Clay Sci. 185, 105416. https://doi.org/10.1016/j.clay.2019.105416.
Lisuzzo, L., Cavallaro, G., Milioto. S., Lazzara, G., 2021. Halloysite nanotubes filled with salicylic acid and sodium diclofenac: effects of vacuum pumping on loading and release properties. J. Nanostruct. Chem. https://doi.org/10.1007/s40097-021-00391-z.
Lisuzzo, L., Cavallaro, G., Pasbakhsh, P., Milioto, S., Lazzara, G., 2019. Why does vacuum drive to the loading of halloysite nanotubes? The key role of water confinement. J. Colloid Interface Sci. 547, 361–369. https://doi.org/10.1016/j.jcis.2019.04.012.

Liu, M., Jia, Z., Jia, D., Zhou, C., 2014. Recent advance in research on halloysite nanotubes-polymer nanocomposite. Prog. Polym. Sci. 39, 1498–1525. https://doi.org/10.1016/j.progpolymsci.2014.04.004.

Maestrelli, F., Zerrouk, N., Cirri, M., Mura, P., 2015. Comparative evaluation of polymeric and waxy microspheres for combined colon delivery of ascorbic acid and ketoprofen. Int. J. Pharm. 485, 365–373. https://doi.org/10.1016/j.ijpharm.2015.02.073.

Mangindaan, D., Chen, C.-T., Wang, M.-J., 2012. Integrating sol–gel with cold plasmas modified porous polycaprolactone membranes for the drug-release of silver-sulfadiazine and ketoprofen. Appl. Surf. Sci. 262, 114–119. https://doi.org/10.1016/j.apsusc.2012.03.003.

Massaro, M., Colletti, C.G., Lazzara, G., Milioto, S., Noto, R., Riela, S., 2017. Halloysite nanotubes as support for metal-based catalysts. J. Mater. Chem. A 5, 13276–13293. https://doi.org/10.1039/C7TA02996A.

Massaro, M., Cavallaro, G., Colletti, C.G., Lazzara, G., Milioto, S., Noto, R., Riela, S., 2018. Chemical modification of halloysite nanotubes for controlled loading and release. J. Mater. Chem. B 6, 3415–3433. https://doi.org/10.1039/C8TB00543E.

de Matos Fonseca, J., de Fátima Medeiros, S., Alves, G.M., Santos, D.M.D., Campana-Filho, S.P., Santos, A., 2019. Chitosan microparticles embedded with multi-responsive poly(N-vinylcaprolactam-co-itaconic acid-co-ethylene-glycol dimethacrylate)-based hydrogel nanoparticles as a new carrier for delivery of hydrophobic drugs. Colloids Surf. B Biointerfaces 175, 73–83. https://doi.org/10.1016/j.colsurfb.2018.11.042.

Oliyaei, N., Moosavi-Nasab, M., Tamaddon, A.M., Fazaeli, M., 2019. Preparation and characterization of porous starch reinforced with halloysite nanotube by solvent exchange method. Int. J. Biol. Macromol. 123, 682–690. https://doi.org/10.1016/j.ijbiomac.2018.11.095.

Rençber, S., Karavana, S.Y., Özyazici, M., 2009. Bioavailability file: Ketoprofen. FABAD J. Pharm. Sci. 34, 203–216.

Rozhina, E., Panchal, A., Akhatova, F., Lvov, Y., Fakhrullin, R., 2020. Cytocompatibility and cellular uptake of alkylsilane-modified hydrophobic halloysite nanotubes. Appl. Clay Sci. 185, 105371. https://doi.org/10.1016/j.clay.2019.105371.

Sabahi, H., Khorami, M., Rezayan, A.H., Jafari, Y., Karami, M.H., 2018. Surface functionalization of halloysite nanotubes via curcumin inclusion. Colloids Surf. A Physicochem. Eng. Asp. 538, 834–840. https://doi.org/10.1016/j.colsurfa.2017.11.038.

Sahnoun, S., Boutahala, M., Zaghouane-Boudiaf, H., Zerroual, L., 2016. Trichlorophenol removal from aqueous solutions by modified halloysite: kinetic and equilibrium studies. Desalination Water Treat. 57, 15941–15951. https://doi.org/10.1080/19443994.2015.1075159.

Sajab, M.S., Chia, C.H., Zakaria, S., Jani, S.M., Ayob, M.K., Chee, K.L., Khiew, P.S., Chiu, W.S., 2011. Citric acid modified kenaf core fibres for removal of methylene blue from aqueous solution. Bioresour. Technol. 102, 7237–7243. https://doi.org/10.1016/j.biortech.2011.05.011.

San Román, M.S., Holgado, M.J., Salinas, B., Rives, V., 2012. Characterisation of diclofenac, ketoprofen or chloramphenicol succinate encapsulated in layered double hydroxides with the hydrotalcite-type structure. Appl. Clay Sci. 55, 158–163. https://doi.org/10.1016/j.clay.2011.11.010.

San Roman, S., Gullón, J., Del Arco, M., Martin, C., 2016. Influence of the surface acidity of the alumina on the sustained release of ketoprofen. J. Pharma. Sci, 105, 2146-2154. https://doi.org/10.1016/j.xphs.2016.04.029.

Schilling, S.U., Bruce, C.D., Shah, N.H., Malick, A.W., McGinity, J.W., 2008. Citric acid monohydrate as a release-modifying agent in melt extruded matrix tablets. Int. J. Pharm. 361, 158–168. https://doi.org/10.1016/j.ijpharm.2008.05.035.

Segovia-Sandoval, S.J., Ocampo-Pérez, R., Berber-Mendoza, M.S., Leyva-Ramos, R., Jacobo-Azuara, A., Medellín-Castillo, N.A., 2018. Walnut shell treated with citric acid and its application as biosorbent in the removal of Zn(II). J. Water Process Eng. 25, 45–53. https://doi.org/10.1016/j.jwpe.2018.06.007.

Tan, D., Yuan, P., Annabi-Bergaya, F., Yu, H., Liu, D., Liu, H., He, H., 2013. Natural halloysite nanotubes as mesoporous carriers for the loading of ibuprofen. Micropor. Mesopor. Mat. 179, 89–98. https://doi.org/10.1016/j.micromeso.2013.05.007.

Tcheumi, H.L., Tassontio, V.N., Tonle, I.K., Ngameni, E., 2019. Surface functionalization of smectite-type clay by facile polymerization of β-cyclodextrin using citric acid cross linker: Application as sensing material for the electrochemical determination of paraquat. Appl. Clay Sci. 173, 97–106. https://doi.org/10.1016/j.clay.2019.03.013.

Tharmavaram, M., Pandey, G., Rawtani, D., 2018. Surface modified halloysite nanotubes: A flexible interface for biological, environmental and catalytic applications. Adv.Colloid Interface Sci. 261, 82–101. https://doi.org/10.1016/j.cis.2018.09.001.

Torres Sànchez, R.M., Basaldella, E.I., Marco, J.F., 1999. The effect of thermal and mechanical treatment on Kaolinite: Characterization by XPS and IEP measurements. J. Colloid Interf. Sci. 215, 339–344. https://doi.org/10.1006/jcis.1999.6241.

Veerabadran, N.G., Price, R.R., Lvov, Y.M., 2007. Clay nanotubes for encapsulation and sustained release of drugs. Nano 02, 115–120. https://doi.org/10.1142/S1793292007000441.

Vergaro, V., Lvov, Y.M., Leporatti, S., 2012. Halloysite claynanotubes for resveratrol delivery to cancer cells. Macromol. Biosci. 12, 1265–1271. https://doi.org/10.1002/mabi.201200121.

Wagner, J.G., 1969. Interpretation of percent dissolved-time plots derived from in vitro testing of conventional tablets and capsules. J. Pharm. Sci. 58, 1253–1257. https://doi.org/10.1002/jps.2600581021.

Xia, M., Liu, H., Wang, H., Sun, F., Zou, X., Chen, T., Chu, Z., Chen, D., Zhou, Y., Xie, Q., 2021. Impact of the interaction between hematite and halloysite on environmental fate of organic pollutants. Appl. Clay Sci. 209, 106123. https://doi.org/10.1016/j.clay.2021.106123.

Yang, H., Zhang, Y., Ouyang, J., 2016. Chapter 4 - Physicochemical Properties of Halloysite, in: Yuan, P., Thill, A., Bergaya, F. (Eds.), Developments in Clay Science, Nanosized Tubular Clay Minerals. Elsevier, pp. 67–91. https://doi.org/10.1016/B978-0-08-100293-3.00004-2.

Yendluri, R., Lvov, Y., de Villiers, M.M., Vinokurov, V., Naumenko, E., Tarasova, E., Fakhrullin, R., 2017a. Paclitaxel encapsulated in halloysite clay nanotubes for intestinal and intracellular delivery. J. Pharm. Sci. 106, 3131–3139. https://doi.org/10.1016/j.xphs.2017.05.034.

Yendluri, R., Otto, D.P., De Villiers, M.M., Vinokurov, V., Lvov, Y.M., 2017b. Application of halloysite clay nanotubes as a pharmaceutical excipient. Int. J. Pharm. 521, 267–273. https://doi.org/10.1016/j.ijpharm.2017.02.055.

Yuan, P., Tan, D., Annabi-Bergaya, F., Yan, W., Fan, M., Liu, D., He, H., 2012. Changes in structure, morphology, porosity, and surface activity of mesoporous halloysite nanotubes underheating. Clays Clay Miner. 60, 561–573. https://doi.org/10.1346/CCMN.2012.0600602.

Zhang, H., Zhou, J., Muhammad, Y., Tang, R., Liu, K., Zhu, Y., Tong, Z., 2019. Citric acidmodifiedbentonite for Congo Red adsorption. Front. Mater. 6, 1–5. https://doi.org/10.3389/fmats.2019.00005.

Zhao, Q., Gao, H., Su, Y., Huang, T., Lu, J., Yu, H., Ouyang, D., 2019. Experimental characterization and molecular dynamic simulation of ketoprofen-cyclodextrin complexes. Chem. Phys. Lett. 736, 136802. https://doi.org/10.1016/j.cplett.2019.136802.

Captions of Figures

Figure 1. Characterization of purified Hal: X-ray diffractogram, Q: quartz, A: alunite (a); FTIR spectrum (b); TEM image (c); N2 adsorption/desorption isotherms (d) and TGA-DTA (e).

Figure 2. X-ray diffractograms of samples.

Figure 3. FTIR spectra of samples (KET, Hal-KET, Hal-CA, Hal-CA-KET).

Figure 4. TEM images of Hal-KET (a); Hal-CA (b) and Hal-CA-KET (c).

Figure 5. N2 adsorption/desorption isotherms of samples.

Figure 6. ATG and DSC thermograms of samples.

Figure 7. Dissolution profiles of KET, KET from Hal and KET from Hal-CA.

Figure 8. Anti-inflammatory activity of KET, Hal-KET and Hal-CA-KET in rats.

Figure 9. Analgesic effect of KET, Hal-KET and Hal-CA-KET on acetic acid-induced writhings in mice. **** $p < 0.0001$ very highly significantly.

Figure 10. Macroscopic findings of KET-induced gastric mucosal lesions. Control (a); KET (b); Hal-KET (c) and Hal-CA-KET (d).

Figure 11. Percentage of KET-induced ulceration (total area of lesions). **** $p < 0.0001$ very highly significantly.

Figure 12. Stomach histopathology: control rats (a_1,a_2); rats treated with KET (b_1-b_4); rats treated with Hal-KET (c_1,c_2) and rats treated with Hal-CA-KET (d_1,d_2). Congestion (**C**), infiltration (**I**), hemorrhagic bands in the gastric mucosa (**H**).

a)

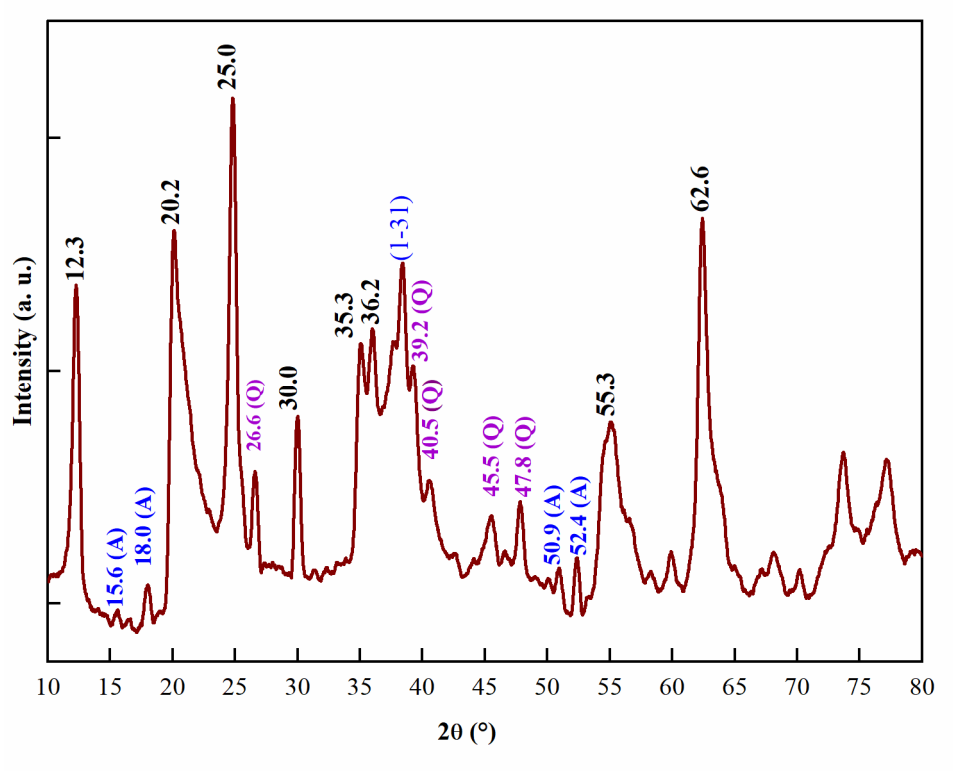
Intensity (a. u.)
2θ (°)
12.3
15.6 (A)
18.0 (A)
20.2
25.0
26.6 (Q)
30.0
35.3
36.2
(1-31)
39.2 (Q)
40.5 (Q)
45.5 (Q)
47.8 (Q)
50.9 (A)
52.4 (A)
55.3
62.6

b)

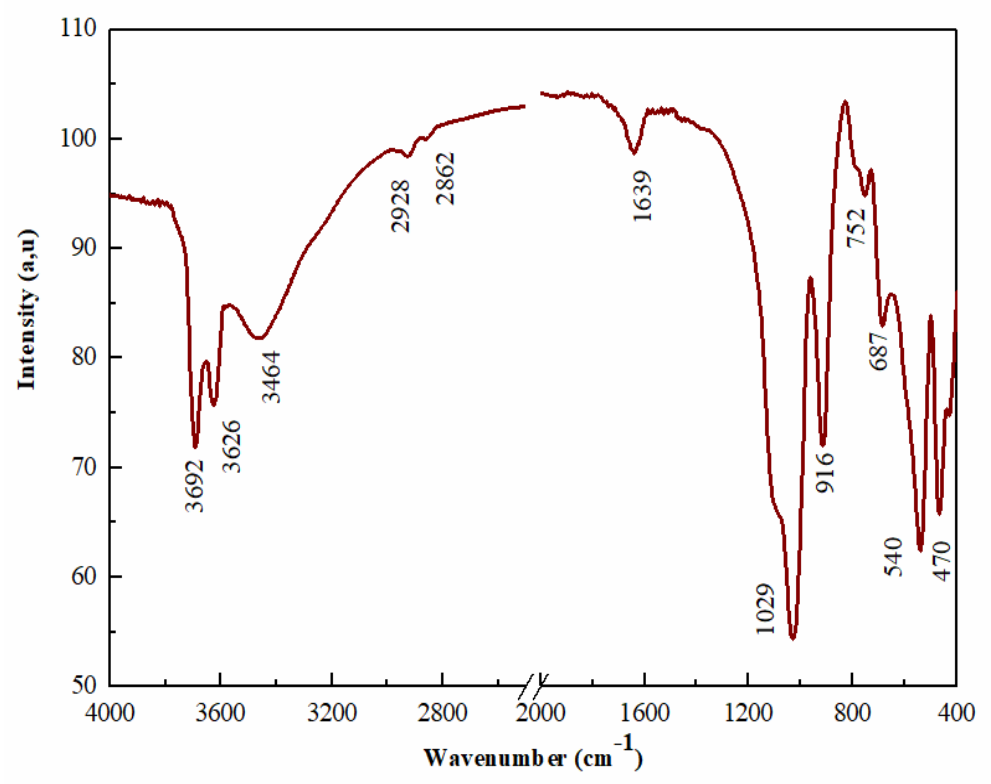
Intensity (a,u)
Wavenumber (cm-1)
3692
3626
3464
2928
2862
1639
1029
916
752
687
540
470

c)

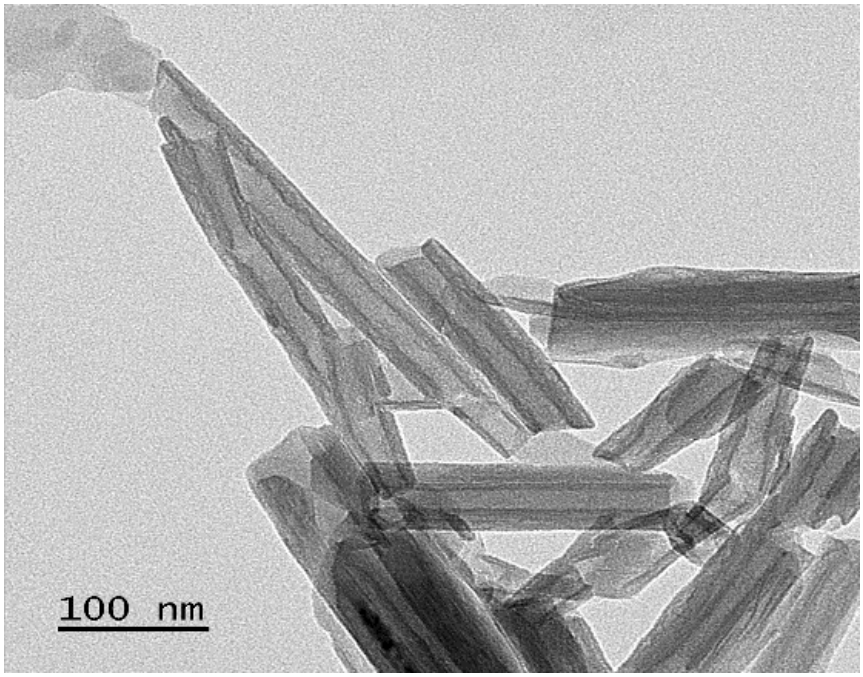
100 nm

d)

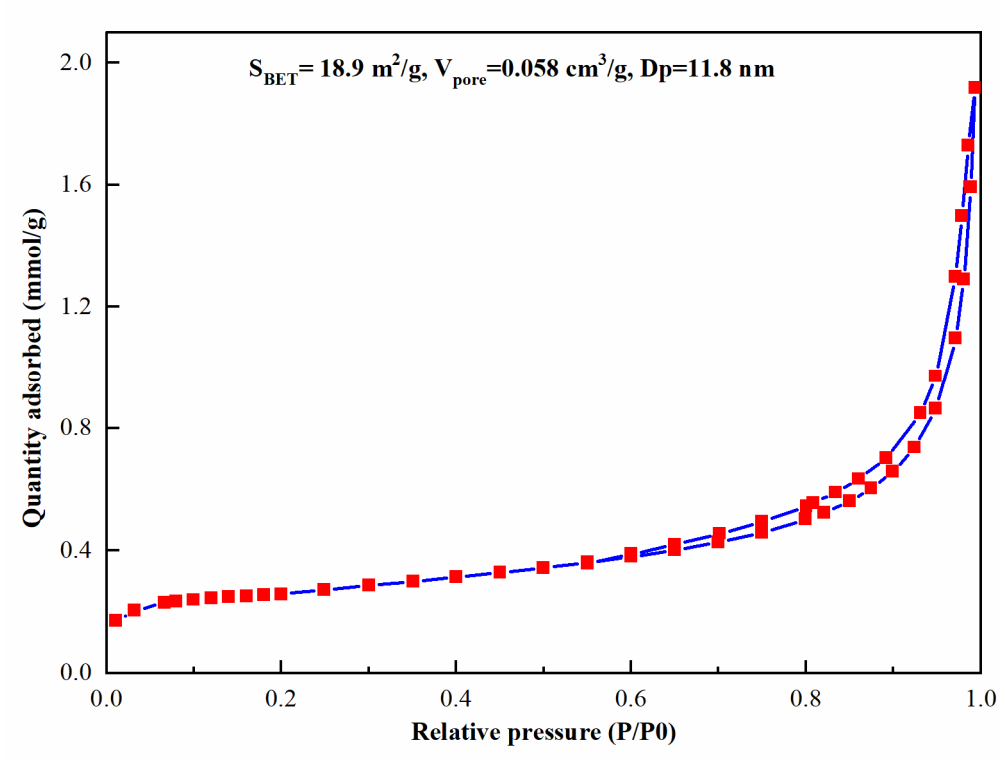
S_BET= 18.9 m²/g, V_pore=0.058 cm³/g, Dp=11.8 nm
Quantity adsorbed (mmol/g)
Relative pressure (P/P0)
0.0
0.4
0.8
1.2
1.6
2.0
0.0
0.2
0.4
0.6
0.8
1.0

e)

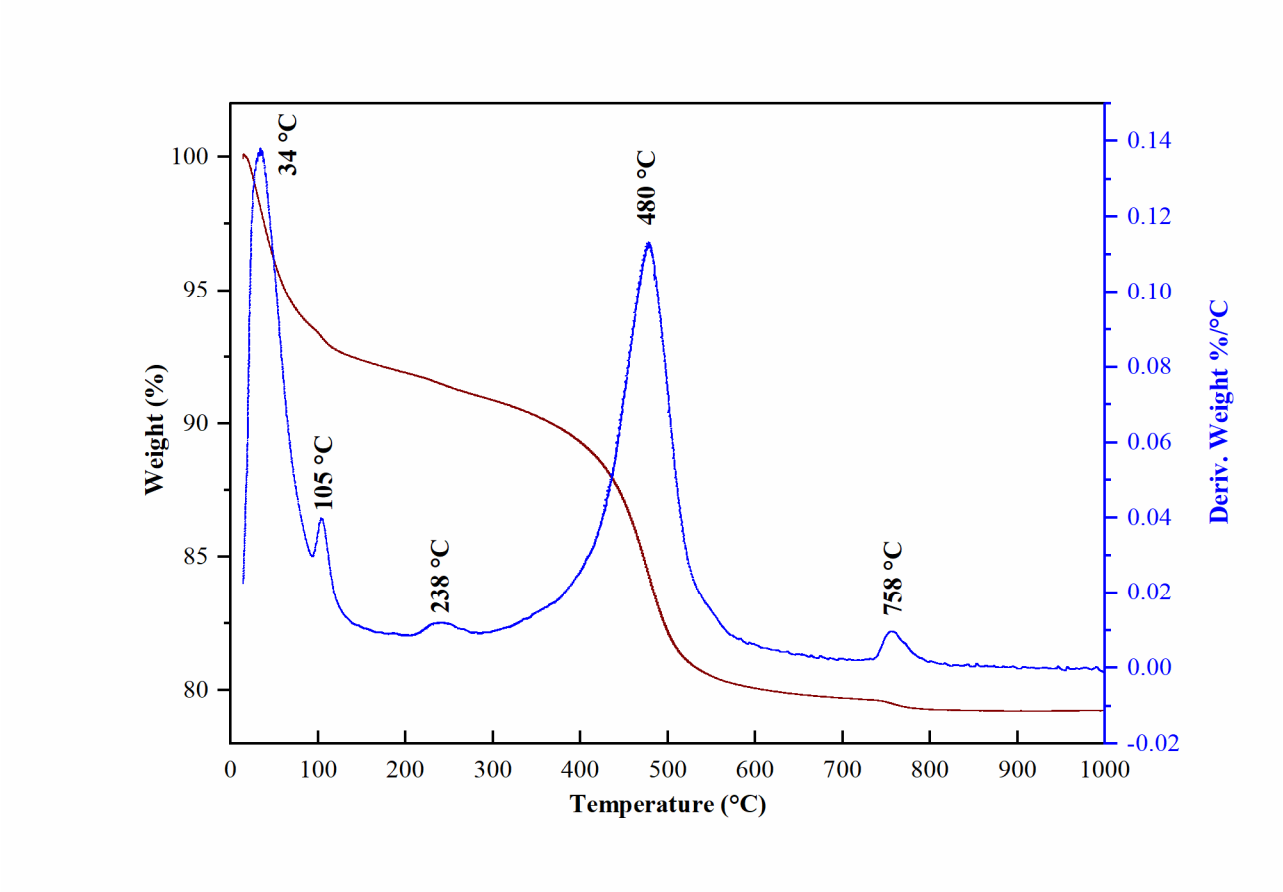
34 °C
105 °C
238 °C
480 °C
758 °C
Weight (%)
Deriv. Weight %/°C
Temperature (°C)
100
95
90
85
80
0
100
200
300
400
500
600
700
800
900
1000
0.14
0.12
0.10
0.08
0.06
0.04
0.02
0.00
-0.02

Fig. 1.

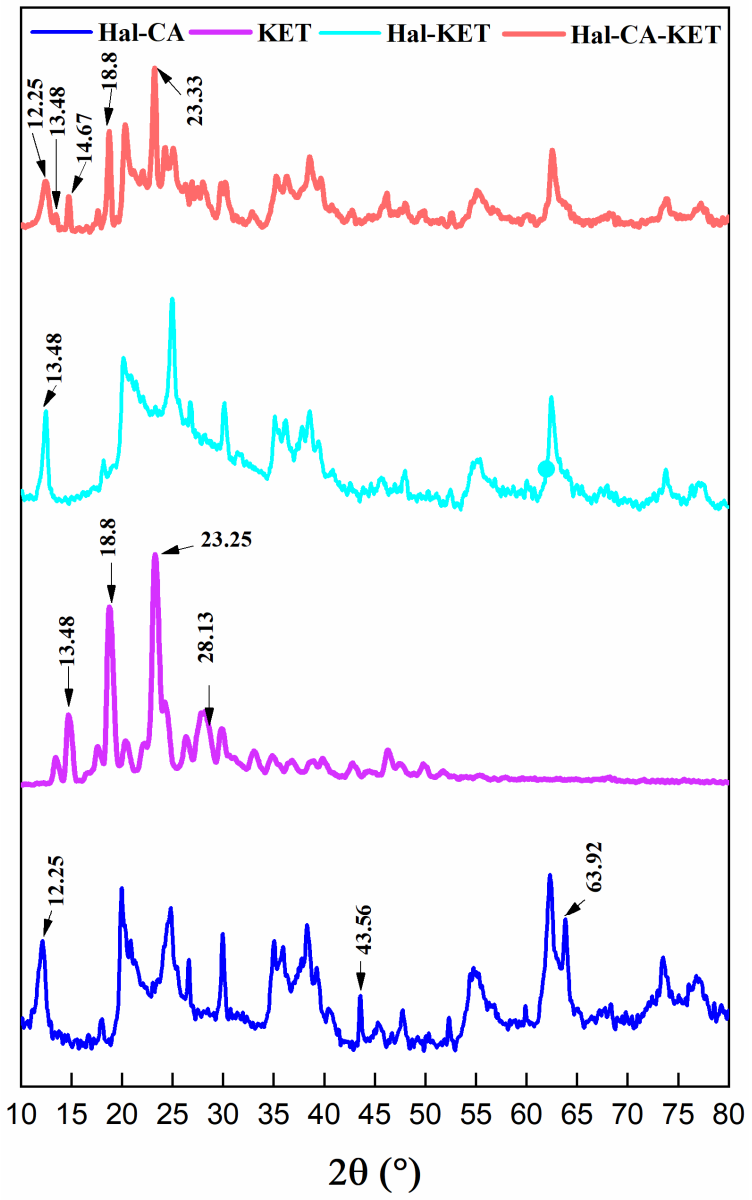
Hal-CA
KET
Hal-KET
Hal-CA-KET
12.25
13.48
14.67
18.8
23.33
13.48
18.8
23.25
13.48
28.13
12.25
43.56
63.92
10 15 20 25 30 35 40 45 50 55 60 65 70 75 80
2θ (°)

Fig. 2.

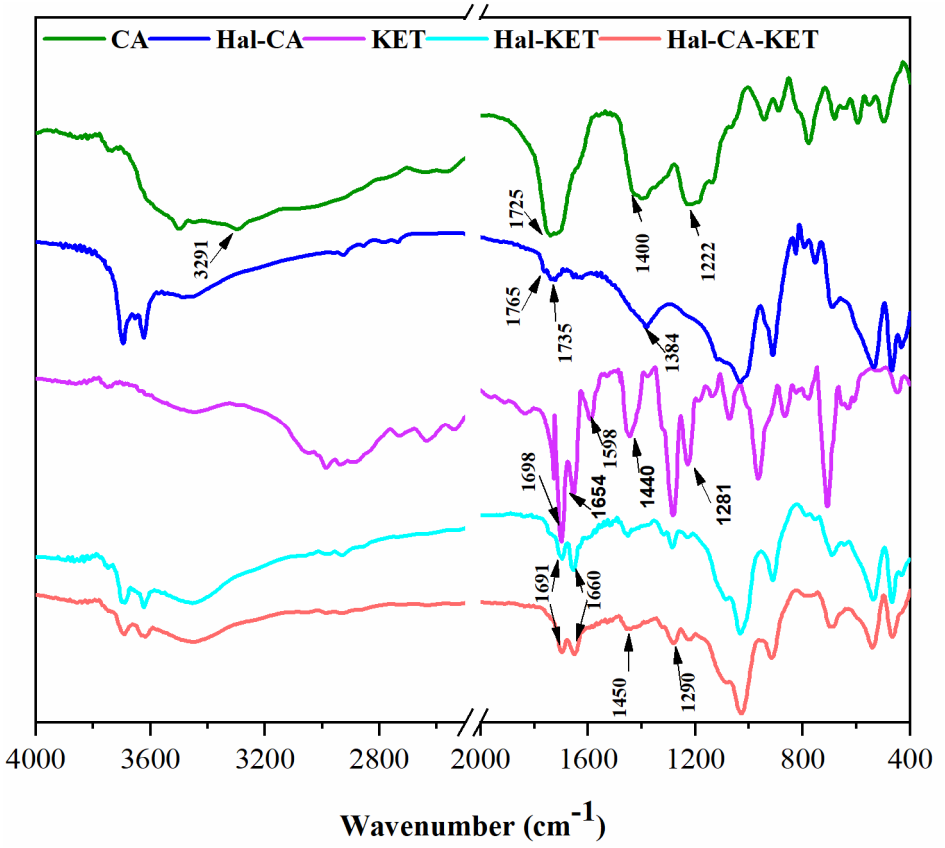
CA
Hal-CA
KET
Hal-KET
Hal-CA-KET
3291
1725
1400
1222
1765
1735
1384
1698
1654
1598
1440
1281
1691
1660
1450
1290
4000
3600
3200
2800
2000
1600
1200
800
400
Wavenumber (cm-1)

Fig. 3.

a)

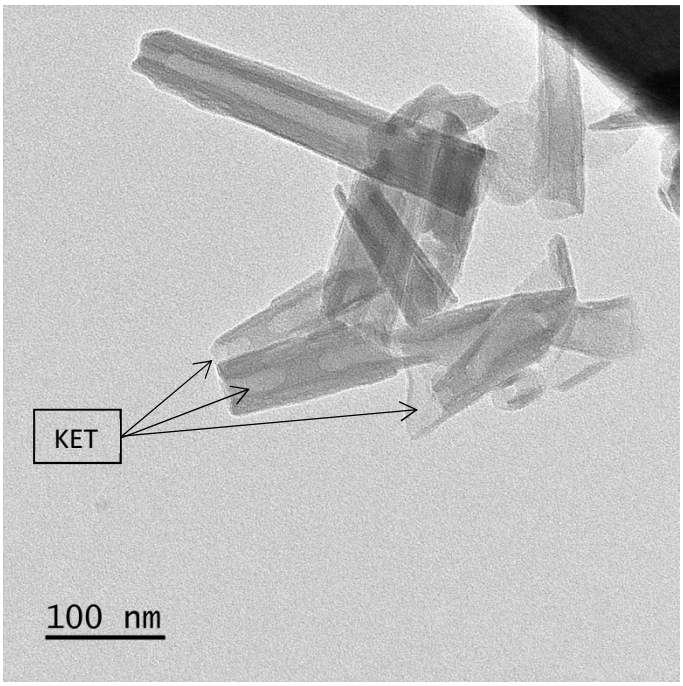

b)

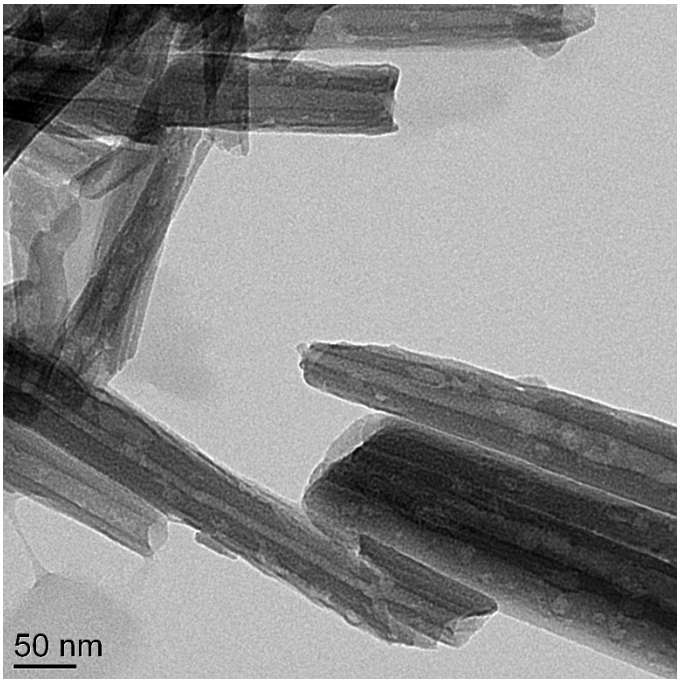

c)

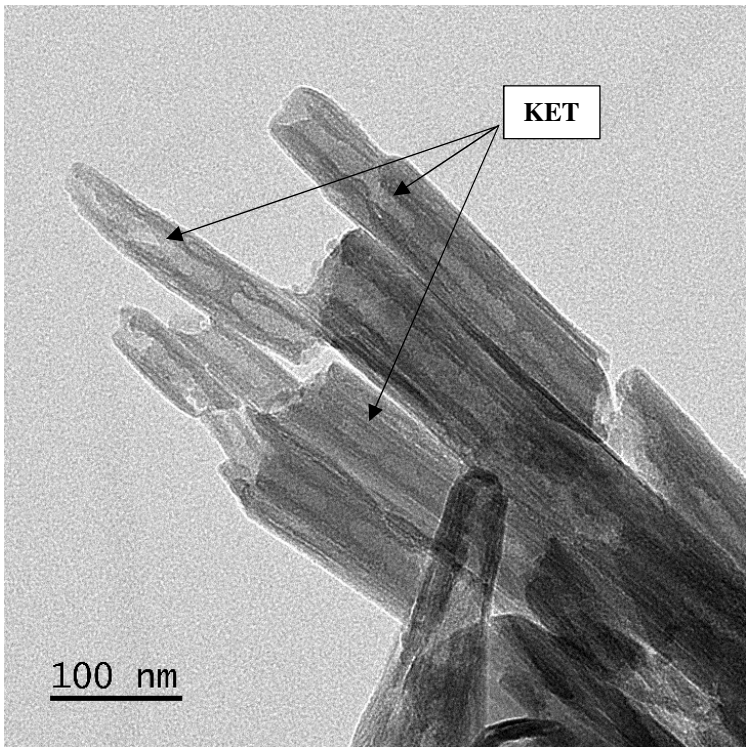

Fig. 4.

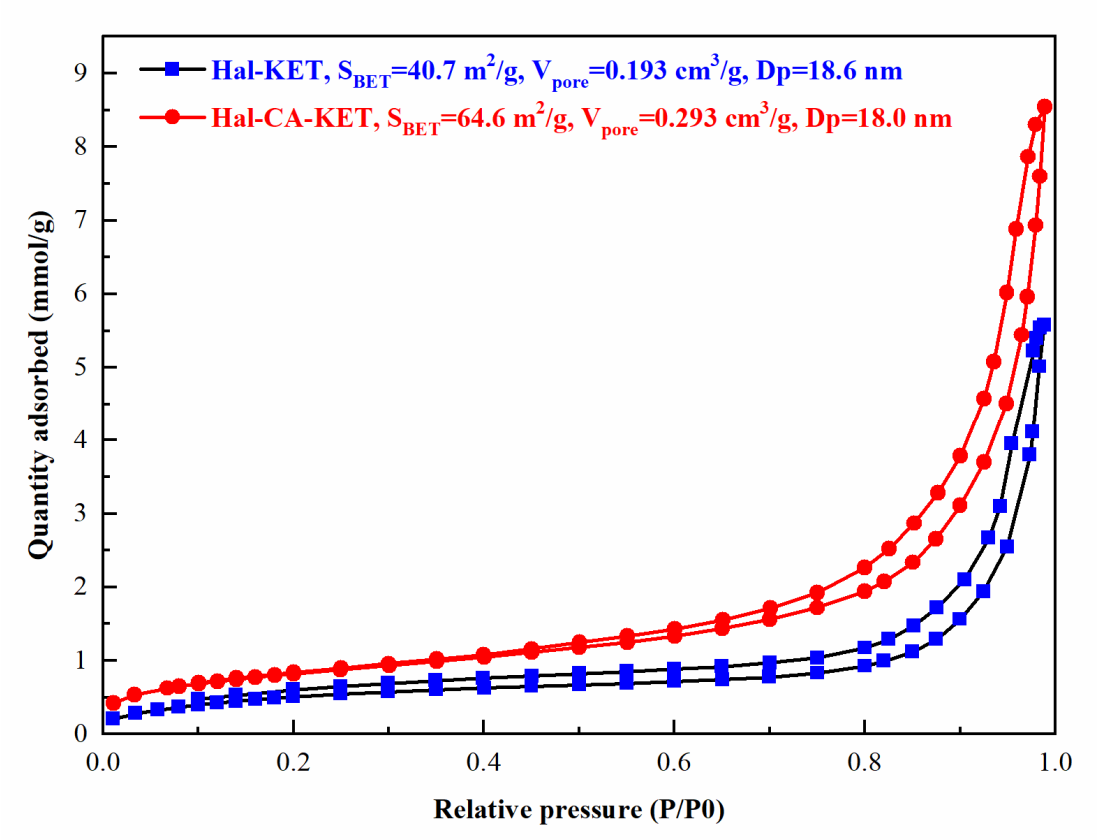
Hal-KET, S_BET=40.7 m²/g, V_pore=0.193 cm³/g, Dp=18.6 nm
Hal-CA-KET, S_BET=64.6 m²/g, V_pore=0.293 cm³/g, Dp=18.0 nm
Quantity adsorbed (mmol/g)
Relative pressure (P/P0)
0
1
2
3
4
5
6
7
8
9
0.0
0.2
0.4
0.6
0.8
1.0

Fig. 5.

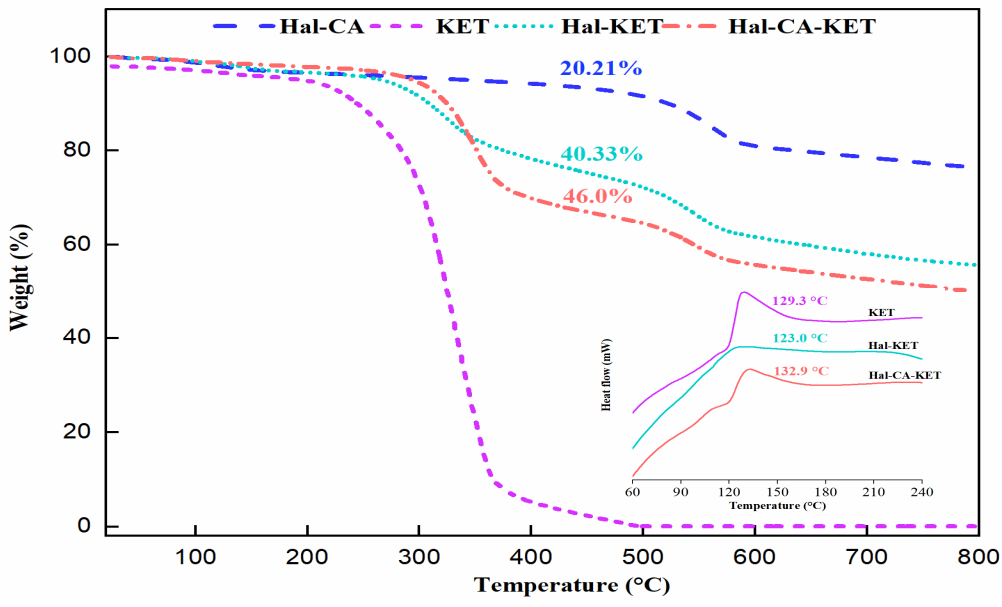
Hal-CA
KET
Hal-KET
Hal-CA-KET
20.21%
40.33%
46.0%
Weight (%)
Temperature (°C)
129.3 °C
123.0 °C
132.9 °C
Heat flow (mW)
Temperature (°C)

Fig. 6.

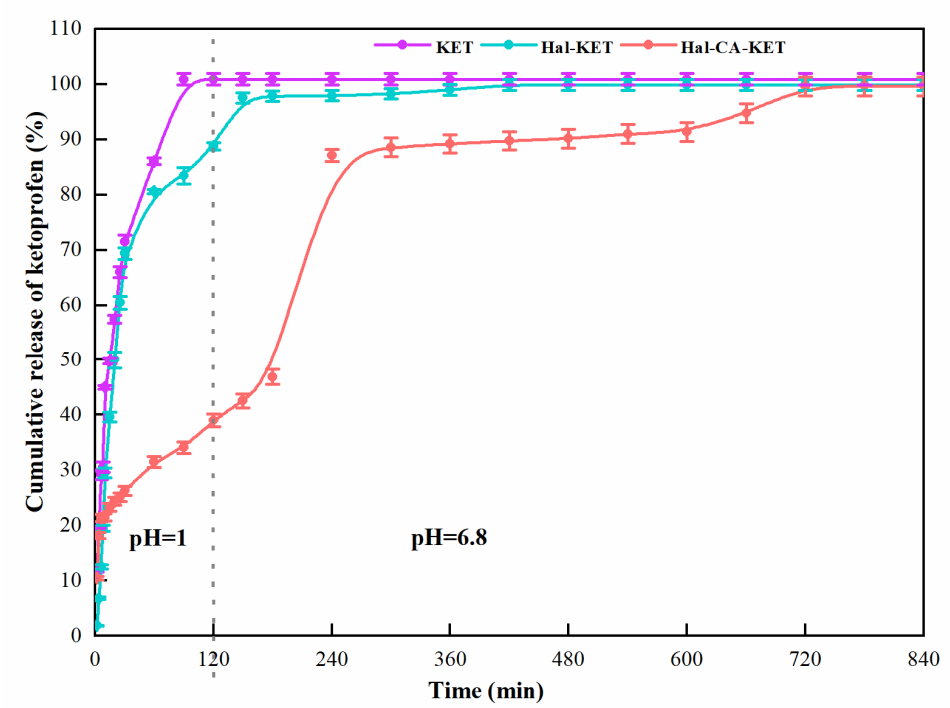
KET
Hal-KET
Hal-CA-KET
Cumulative release of ketoprofen (%)
pH=1
pH=6.8
Time (min)

Fig. 7.

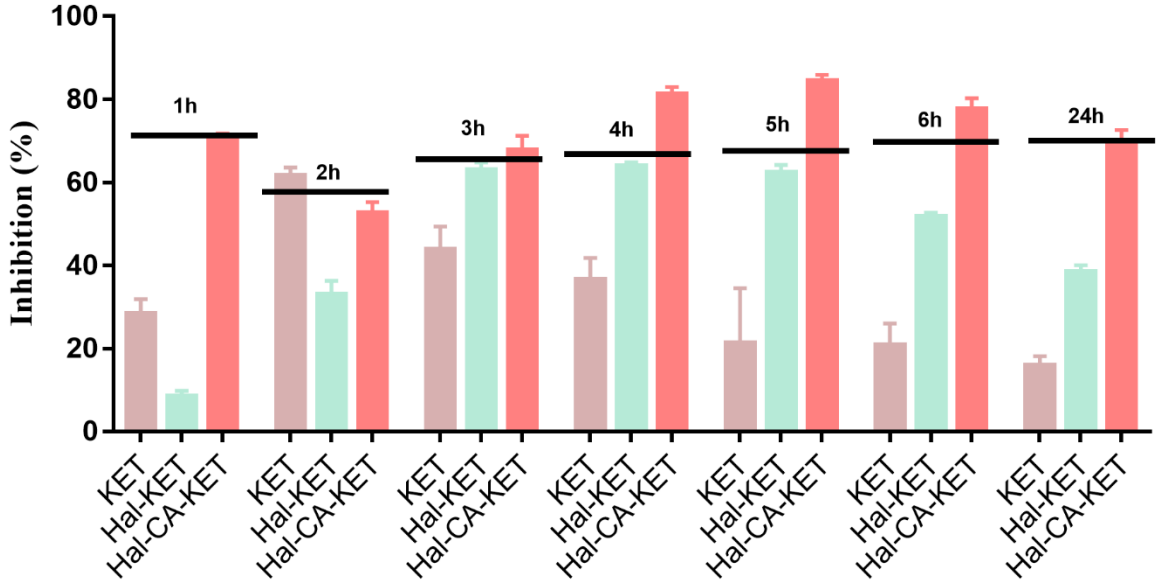
Inhibition (%)
100
80
60
40
20
0
1h
2h
3h
4h
5h
6h
24h
KET
Hal-KET
Hal-CA-KET

Fig. 8.

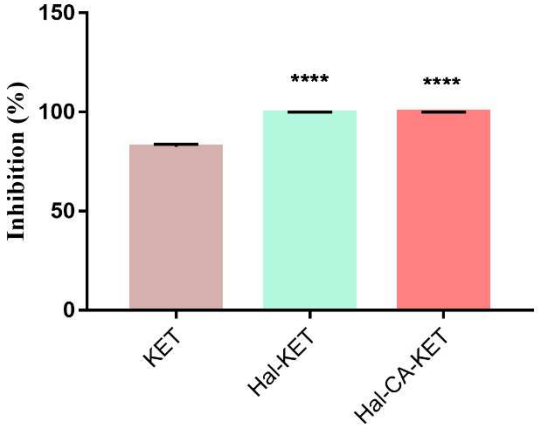
Inhibition (%)
150
100
50
0
****
****
KET
Hal-KET
Hal-CA-KET

Fig. 9.

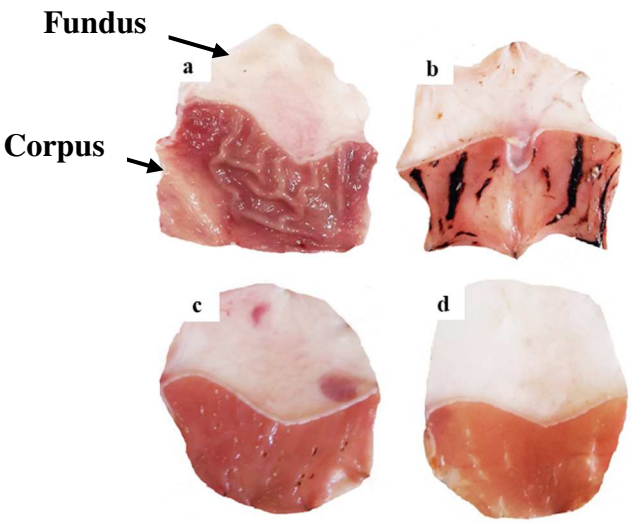

Fig. 10.

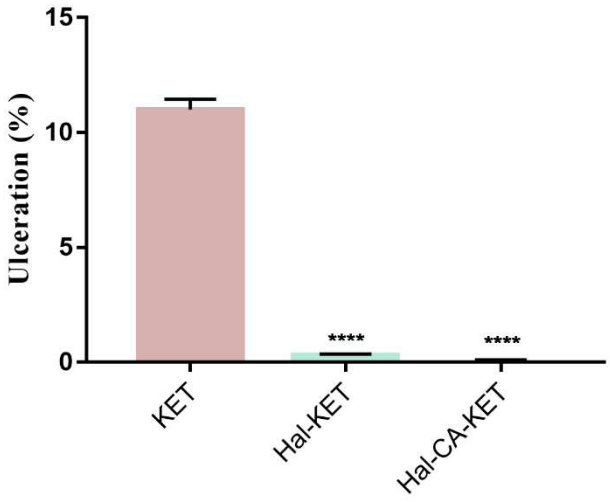

Fig. 11.

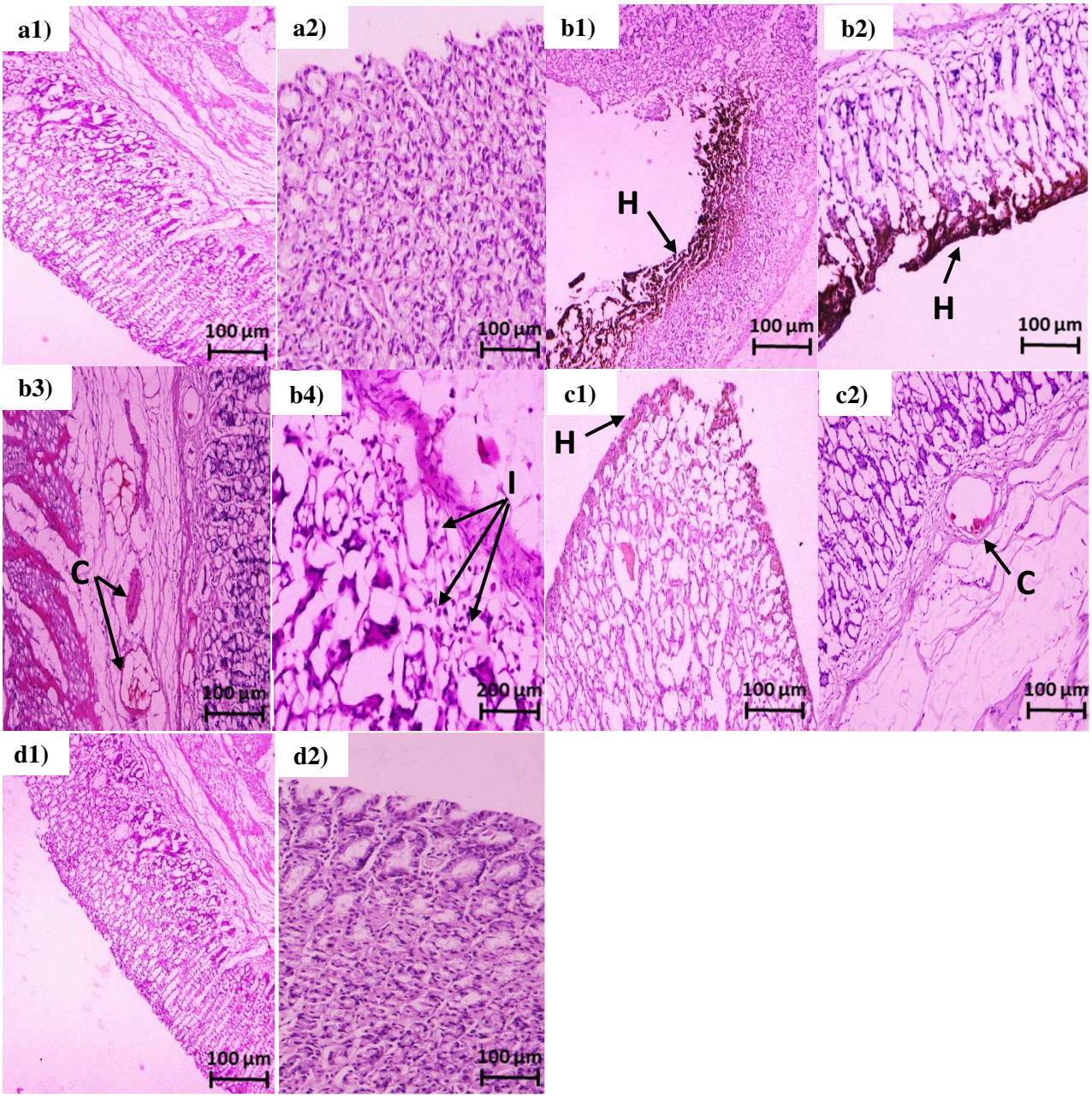
a1)
100 µm
a2)
100 µm
b1)
H
100 µm
b2)
H
100 µm
b3)
C
100 µm
b4)
I
200 µm
c1)
H
100 µm
c2)
C
100 µm
d1)
100 µm
d2)
100 µm

Fig. 12.

Captions of Tables

Table 1: *In vivo* ulcerogenicity activity experiment design.

Table 2: Release parameters for formulations obtained after data fitting with Korsmeyer–Peppas model of drug release kinetics.

Table 1

Groups (n=6)	Treatment	Dose (mg·kg^{-1}) of KET
I	Control (saline)	-
II	Pure KET	500
III	Hal-KET	500
VI	Hal-CA-KET	500

Table 2

	Sample	K_{KP}	n	R^2
pH=1	Hal-KET	0.104±0.0271	0.473±0.0637	0.900
	Hal-CA-KET	0.115±0.0078	0.248±0.0177	0.981
pH=6.8	Hal-KET	0.899±0.0130	0.0161±0.0018	0.870
	Hal-CA-KET	0.116±0.0617	0.327±0.071	0.973

Graphical Abstract